Amelin
Journal of Analytical Science and Technology (2024) 15:22
https://doi.org/10.1186/s40543-024-00435-3

Journal of Analytical Science and Technology

REVIEW

Open Access

Sample size and the limits to precision in Pb-isotopic dating by ID-TIMS

Yuri Amelin[1*]

Abstract

Using isotope analysis of ancient (4555 Ma) radiogenic Pb by ID-TIMS as an example, I evaluate the sample size required to achieve the target precision of the $^{207}Pb/^{206}Pb$ ratio 0.007% (2σ), corresponding to the uncertainty of the $^{207}Pb^*/^{206}Pb^*$ age of 0.1 million years, considering various analytical uncertainties. In a hypothetical perfect analytical setup that would enable measuring isotopic ratios without noise, losses and biases, this precision can be achieved by analysis of a sample containing 2.9 picograms of Pb. Assessment of the sources of noise, loss and bias introduced by sample preparation and mass spectrometry shows that incomplete ionization of Pb during evaporation from the filament and baseline noise of a mass spectrometer make the greatest contributions to the additional uncertainty. Subtraction of analytical blank and minor spike isotopes can also substantially increase the uncertainty under some analytical conditions. The contributions from the other sources are smaller, but can become significant if a higher precision level is sought.

Introduction

Samples of geological and extraterrestrial materials are often available only in small quantities, and this sample size restriction constrains precision of their isotope analysis. Specimens of extraterrestrial rocks delivered by sample return space missions, mineral inclusions in other mineral grains, individual mineral grains, fluid inclusions, and components of rare meteorites are just a few examples among the innumerable materials that could have been analyzed more precisely if they were larger. Increasing sample sizes for these materials is either impossible due to limited availability, or is prevented by the need to resolve the internal heterogeneity of the samples. At the same time, the requirements to precision of isotope analysis are becoming more demanding because of the need to resolve smaller natural isotopic variations (in isotope geochemistry) and shorter time intervals (in geochronology).

*Correspondence:
Yuri Amelin
yuri.amelin@anu.edu.au
[1] Korea Basic Science Institute, Ochang, South Korea

Like any isotope analyses in geochemistry and geochronology, Pb-isotope analyses in U–Pb geochronology are burdened by multiple sources of uncertainty. In this paper, I discuss precision in isotope analysis in Pb-isotopic dating of meteorites and ancient rocks using radiogenic $^{207}Pb^*/^{206}Pb^*$ ratio as an example. I review the limits to precision imposed by the sample size, the additional sources of uncertainty of isotopic ratios, their comparative significance and possible ways of minimization.

What precision of the isotopic dates do we need?

This question is meaningful for a chemist who develops analytical methods for earth science or some other area of research. For a geochemist, however, the obvious answer is "the higher precision the better". Any improvement in precision can be utilized to solve a broader range of geological and cosmochemical problems by isotopic dating. The best precision achieved in a single measurement of the $^{207}Pb/^{206}Pb$ ratio in modern Pb-isotopic dating for meteorites and their components that are sufficiently large and homogeneous is about ± 0.1–0.2 Ma (e.g., Amelin 2008a, b; Connelly et al. 2012, 2023; Krestianinov et al. 2023) at 2σ level, which is used throughout this paper unless indicated otherwise. In this study, I

Springer Open

© The Author(s) 2024. **Open Access** This article is licensed under a Creative Commons Attribution 4.0 International License, which permits use, sharing, adaptation, distribution and reproduction in any medium or format, as long as you give appropriate credit to the original author(s) and the source, provide a link to the Creative Commons licence, and indicate if changes were made. The images or other third party material in this article are included in the article's Creative Commons licence, unless indicated otherwise in a credit line to the material. If material is not included in the article's Creative Commons licence and your intended use is not permitted by statutory regulation or exceeds the permitted use, you will need to obtain permission directly from the copyright holder. To view a copy of this licence, visit http://creativecommons.org/licenses/by/4.0/.

accept the precision of measurement of the $^{207}Pb^*/^{206}Pb^*$ ratio of 0.007% (Pb* denotes radiogenic Pb), which corresponds to precision of the age of 0.1 Ma for materials older than ~ 4500 Ma, as a significance threshold in the following discussion of the interplay between uncertainties, sample size, and the factors that complicate isotopic analyzes. By combining several sample analyses with individual precision of the $^{207}Pb/^{206}Pb$ ratio of ca 0.007% in an isochron regression or as a weighted mean of model dates, we can achieve precision of the age of ~ 0.05 Ma or possibly higher, which slightly exceeds the state-of-the-art of modern Pb-isotopic dating. While higher precision of individual analyzes is certainly desirable, it is also likely to also reveal more complexities in isotope systematics (Amelin et al. 2009), which have to be accounted for to achieve the accuracy that matches precision. Since complexities that could cause systematic uncertainties in Pb-isotope analysis with precision < 0.007% are only partially known (e.g., mass-independent component of isotope fractionation during TIMS analysis) and are incompletely understood, the prospect of achieving the highest possible precision of Pb isotope analysis is considered to be beyond the scope of this paper, and is not discussed here. Instead, this paper focuses on the possibility of reducing sample size while maintaining the precision of the $^{207}Pb^*/^{206}Pb^*$age around 0.1 Ma, and analytical developments necessary to achieve this sample size reduction.

Relationship between precision of isotopic ratios, sample size, and performance of the analytical procedure

The ultimate limit on precision of the abundance ratio of isotopes A and B of some element (an analyte hereafter) is defined by the number of atoms of the isotopes of interest that are present in the sample. If we could convert all these atoms into ions, and count these ions using a perfectly accurate and noise-free mass spectrometer, then the relative standard deviation $\sigma(A/B)$ of the isotopic ratio A/B would be given by counting statistics (e.g., Zou 2014):

$$\sigma(\mathrm{A}) = \left(\sqrt{\mu(\mathrm{A})}\right)/\mu(\mathrm{A}) = 1/\sqrt{\mu(\mathrm{A})} \quad (1)$$

$$\sigma(B) = \left(\sqrt{\mu(B)}\right)/\mu(A) = 1/\sqrt{\mu(B)} \quad (2)$$

$$\sigma(A/B) = \sqrt{(\sigma(A)^2 + \sigma(B)^2)} \quad (3)$$

where $\mu(A)$ and $\mu(A)$ are numbers of atoms of the isotopes A and B, respectively. If we analyze Pb with atomic abundances of $^{206}Pb = 25\%$ and $^{207}Pb = 15.5\%$ (corresponding to $^{207}Pb/^{206}Pb = 0.62$, a single-stage radiogenic composition from a 4555 Ma source with $^{238}U/^{235}U = 137.79$) under these perfect conditions, it would require 2.9 pg of Pb to achieve this precision at 2σ level, or 0.73 pg to achieve this precision at 1σ level.

In practice, the isotopic ratios that we measure are always burdened with additional uncertainty that has two fundamental causes: (1) the number of detected ions is smaller than the atoms that were present in the sample, and (2) noises and biases introduced by the measurement procedures and instrumentation. Any loss of atoms of the analyte during sample preparation and analysis would reduce the number of ions available for counting:

$$\nu(A) = \mu(A) * x \quad (4)$$

$$\nu(B) = \mu(B) * x \quad (5)$$

where x is the total yield of the procedure—ions measured per atoms present in the sample, the measure of effectiveness of analyte utilization following Birck (2001) and Schaltegger et al. (2015).

The total yield is a product of partial (ion or atom) yields x1, x2, etc., for all steps of sample processing and analysis. The value of the total yield and any of the partial yields can be anywhere between 0 and 1. The expressions for the relative standard deviation for a procedure with non-unity yield are:

$$\sigma'(A) = 1/\sqrt{\nu(A)} = 1/\sqrt{(\mu(A) * x)} \quad (6)$$

$$\sigma'(B) = 1/\sqrt{\nu(B)} = 1/\sqrt{(\mu(B) * x)} \quad (7)$$

$$\sigma'(A/B) = \sqrt{(\sigma'(A)^2 + \sigma'(B)^2)} \quad (8)$$

The higher the total yield, the closer the value $\sigma'(A/B)$ from Eq. 8 is to the value $\sigma(A/B)$ from Eq. 3. If the total yield is equal to 1, then Eqs. 6–8 are reduced to Eqs. 1–3. In practice, x is always substantially lower than 1. If, for example, $x = 0.01$, the number of counted ions is 100 times lower than the number of initially available atoms (i.e., 99% atoms were lost during analysis), then the relative uncertainty due to counting statistics is 10 times larger than in the analysis of the same sample with no loss ($x = 1$). In many types of analysis, the total yield is lower than 0.01, and the increase of relative uncertainty due to atom or ion loss is even greater. In the following sections, I will evaluate all steps of the Pb–Pb dating procedure for loss of the analyte atoms and possible ways to minimize this loss.

Noise and biases introduced by imperfect performance of analytical procedures and instrumentation further increase the total uncertainty of isotopic ratios. Each step of sample processing and isotopic ratio measurement contributes an additional random uncertainty,

either directly or through correction of systematic uncertainties, which is in turn always imperfect and uncertain to some extent. The total relative uncertainty $\Sigma(A/B)$ including analytical noise and bias components can be expressed as

$$\Sigma(A/B) = \sqrt{(\sigma'(A/B)^2 + z1^2 + z2^2 + \cdots + zn^2)} \quad (9)$$

where $z1$, $z2$, etc., are uncertainties introduced by various sources of noise and bias. It is assumed that all these sources of noise and bias are independent from each other and hence can be combined quadratically.

Uncertainties from some noise components can be readily quantified. For example, the effect of the amplifier noise can be calculated following the approach of Ludwig (1986) for single collector measurements and Ludwig (1997) for multicollector measurements, as a sum of uncertainties from dark noise on the peak (Eq. 10) and on the background (Eq. 11) for each peak:

$$z1^2 = N^2/\left(P^2 * T1\right) \quad (10)$$

$$z2^2 = N^2/\left(P^2 * T2\right) \quad (11)$$

where $z1^2$ and $z2^2$ fractional variances (i.e., variances divided by the square of the mean of the value measured), N is dark noise in A/s, P is ion beam intensity in A, and $T1$ and $T2$ are integration times (s) on the peak and on the background, respectively. These noise-related uncertainties can be entered into Eq. 9 for calculation of the total uncertainty. The uncertainties from other sources are more complex, especially if they contain both random and systematic components, such as subtraction of analytical blanks and correction of instrumental mass fractionation.

Below, I provide a semi-quantitative evaluation of each of the sources of noise and bias in Pb–Pb dating by ID-TIMS. A quantitative model that accounts for uncertainty correlations would be desirable, although the development of such a model is beyond the scope of this paper. However, there are two reasons why it can be expected that the results of the simple evaluation presented here are likely to be comparable to the results from a quantitative model. First, most sources of uncertainty are introduced by different steps of sample preparation and analysis, and are independent and hence uncorrelated. Second, the biggest uncertainty in error evaluation comes from the uncertainty of input parameters, or from omission of possibly significant uncertainty components, rather than from the model. Therefore, I think that the simple but comprehensive semi-quantitative assessment of uncertainties presented here is expected to provide a reasonable guidance for the future analytical developments.

Maximizing the number of detected ions

In Pb-isotopic dating by ID-TIMS, each fraction (e.g., a fragment of a rock or its component, such as a chondrule or Ca-Al-rich inclusion, or a mineral fraction consisting of one or more mineral grains and/or fragments), is separated from host rock, cleaned by some mechanical and/or chemical means, spiked, dissolved, and put through some chemical separation procedure to extract Pb and U that are sufficiently pure for isotopic analysis with TIMS. The separated elements are loaded on metal filaments, and ionized in a mass spectrometer. The ions that reach collector are registered by an analog beam current measuring device (such as a Faraday cup connected to an electrometer amplifier), or counted with a secondary electron multiplier or a Daly detector.

Loss of Pb* during sample preparation

In evaluation of the Pb yield in sample preparation for isotopic dating, we have to consider two factors. The first is the direct loss during sample dissolution and chemical separation of Pb. In carefully executed modern dissolution and separation procedures, these losses are minimal. If all minerals in the sample are completely decomposed during dissolution in hydrofluoric acid (using, if necessary, high-temperature, high-pressure bombs, Krogh 1973), and formation of insoluble fluorides is prevented (Yokoyama et al. 1999), then the loss of Pb during sample dissolution is insignificant.

Likewise, the commonly used procedures of anion exchange separation of Pb where the sample is loaded, and the major elements are removed, in dilute hydrobromic acid (Korkisch and Hazan 1965; Strelow and Toerien 1966) have very high yields. Due to high distribution coefficients > 1000 for Pb between anion exchange resin (AG1 × 8) and 0.1–0.5 M HBr solutions (Guseva 2007), modern column separation procedures have Pb yields of about 97–98% (Kamber and Gladu 2009), while maintaining low blanks and effective separation of matrix elements. The loss of Pb during properly tested dissolution and anion exchange separation procedures is therefore negligible and does not measurably contribute to the uncertainty expansion.

The second potential cause of Pb-loss is the need to eliminate parts of the sample with disturbed or contaminated U–Pb systems. This is achieved by procedures such as chemical abrasion in zircon dating (Mattinson 2005, 2011; Mundil et al. 2004), and multistep partial dissolution of meteorites (Amelin and Krot 2007; Connelly and Bizzarro 2009). When we use these procedures, we seek a balance between maximizing the amount of Pb* available

for analysis, and keeping the geochemical system clean, simple, and closed.

Chemical abrasion of zircon exists in two versions. The first one is the procedure of Mattinson (2005, 2011) where a multigrain fraction is sequentially leached in several portions of HF with increasing temperature, concentration and/or time. In this procedure, all step leachates are analyzed, and all radiogenic Pb is accounted for. This procedure is extremely effective at removing zircon material that experienced loss of radiogenic Pb, but unfortunately it gives accurate age only for zircon populations that are completely free from inherited or xenocrystic components. Therefore, it is not applicable to timescale geochronology of felsic volcanic rocks where zircon grains that pre-date eruption are commonly present. The second is the single-grain version of chemical abrasion, pioneered by Mundil et al. (2004) and now universally adopted by the geochronology community. Single-grain chemical abrasion allows effective detection of pre-eruption zircon components (cores, xenocrysts and antecrysts), but because the amount of U and Pb* in a single zircon grain is small, usually only one leaching step is performed, and only the residue is analyzed. Evaluation of the loss of Pb* in such procedure is difficult. However, in the study of conditions of zircon chemical abrasion by Huyskens et al. (2016) single grains of three zircon reference materials were subjected to two steps of HF leaching before dissolution, and the last step leachate was analyzed for U–Pb along with the residue. The distribution of Pb* in leachate-residue pairs (Fig. 1) demonstrates that between 53 and 98% of Pb is contained in the residue, with the mean value of 85 ± 10%, with almost no dependence on the age of the zircon and conditions of leaching. These data demonstrate that the loss of Pb* in the modern single grain chemical abrasion is in most cases not a significant problem, and does not measurably enlarge the uncertainty.

In U–Pb chronometry of meteorites, it is rarely possible to extract and analyze minerals that contain U and radiogenic Pb, but no other Pb components. More commonly, an age determination is based on a $^{207}Pb/^{206}Pb$ versus $^{204}Pb/^{206}Pb$ isochron regression for a series of fractions containing various proportions of single-stage radiogenic Pb and initial Pb, but no other Pb components. Such a regression satisfies the requirements of the isochron model, and, if the other input parameters and corrections (e.g., blank subtraction, $^{238}U/^{235}U$, half-lives, etc.) are accurate, it yields an accurate $^{207}Pb^*/^{206}Pb^*$ age (e.g., Amelin et al. 2005a; Connelly et al. 2017). In the absence of initial Pb, a binary mixture of Pb* and one other homogeneous Pb component (e.g., contaminant Pb) can also yield an accurate isochron age. Multistep acid leaching of meteorites and their components is

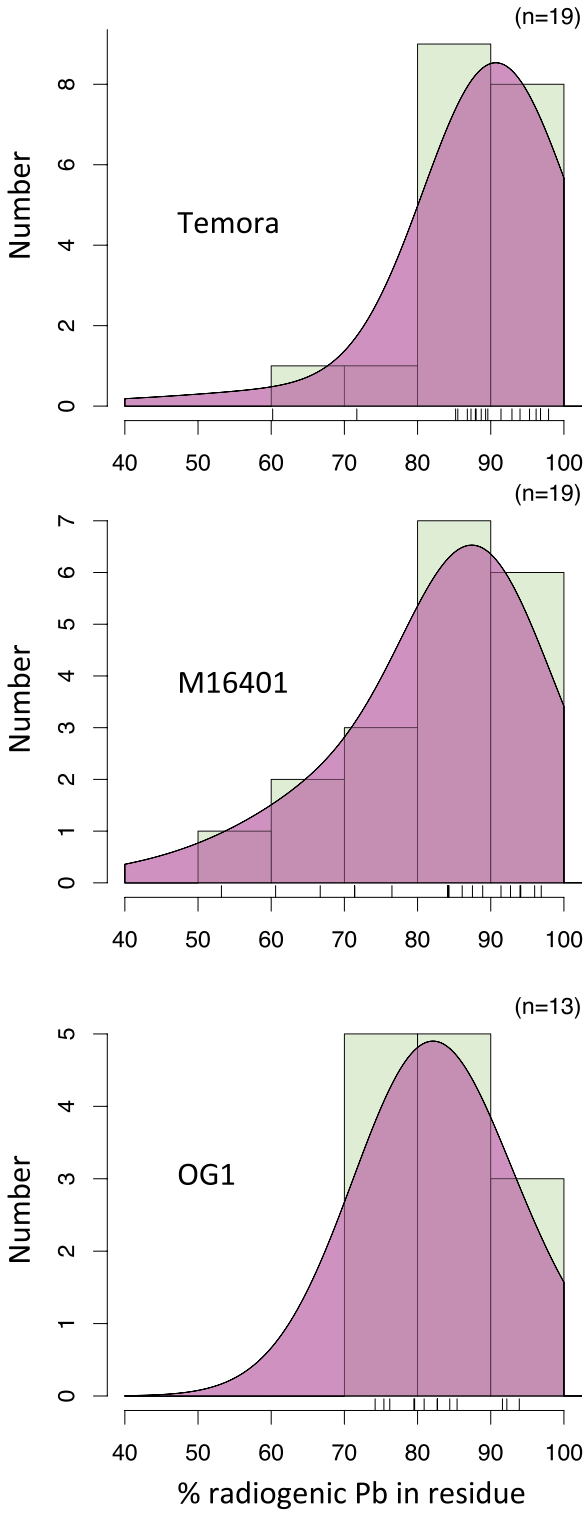

Fig. 1 Distribution of radiogenic Pb between HF leachates and residues of single grains of zircon reference materials Temora, M16401, and OG1, based on the data in Table 1 of Huyskens et al. 2016. X scale shows the percentage of the total Pb* in leachate-residue pairs contained in the residue. Y-scale shows the number of zircon grains within each distribution bin

intended to reduce a natural mixture of multiple Pb components with various origins and isotopic compositions to a binary Pb isotopic mixture.

Effectiveness of multistep leaching varies greatly depending on the composition and mineralogy of the extraterrestrial material. In favorable cases where the meteorite or its component is enriched in U and/or depleted in non-radiogenic Pb, and the solubility of minerals containing different Pb components in acids varies substantially, a simple 2–3 step leaching in HNO_3 and HCl is sufficient to reduce contaminant Pb in the residue below the detection limit, and to produce a binary mixture of nearly pure radiogenic Pb and a small amount of initial Pb of primordial isotopic composition (Tatsumoto et al. 1973; Blichert-Toft et al. 2010). Many, although not all, achondrites, and Ca-Al-rich refractory inclusions belong to this category. The magnitude of loss of radiogenic Pb during step leaching is illustrated by the data for ungrouped achondrites Erg Chech 002 (Krestianinov et al. 2023) and Northwest Africa (NWA) 6704 (Amelin et al. 2019), shown in Figs. 2 and 3, respectively. Between ca. 40% and 80% of radiogenic Pb in pyroxene and whole rock is located in the residues, which typically contain the most radiogenic Pb (at least in the absence of HF leaching steps), and are the primary data for obtaining precise isochron age. The radiogenic Pb that is present in the earlier leaching steps can be considered an inevitable loss of the current step leaching procedures, because these leachates usually contain three or more Pb components (radiogenic, initial, and one or more contaminants), and cannot be included in isochron regressions. This loss corresponds x between 0.4 and 0.8 in Eqs. 4–8 and translates into a ca. 1.1–1.6 times increase of the uncertainty component related to counting statistics.

Some meteorite components, such as chondrules, often contain more abundant non-radiogenic Pb that is also spread among various minerals, so obtaining the data usable for calculation of precise Pb–Pb ages requires more extensive and more aggressive leaching procedures (Connelly and Bizzarro 2009; Bollard et al. 2017). In the most difficult cases, non-radiogenic Pb is both pervasive and resilient to acid leaching, and even the procedure with up to 12 leaching steps, including 5 steps of HF leaching, would create only a small spread of the Pb–Pb isochron (Merle et al. 2020). Dating such stubborn rocks would greatly benefit from development of alternative procedures that would separate mineral phases that predominantly contain radiogenic or non-radiogenic Pb components by other physical or chemical properties, e.g., volatility.

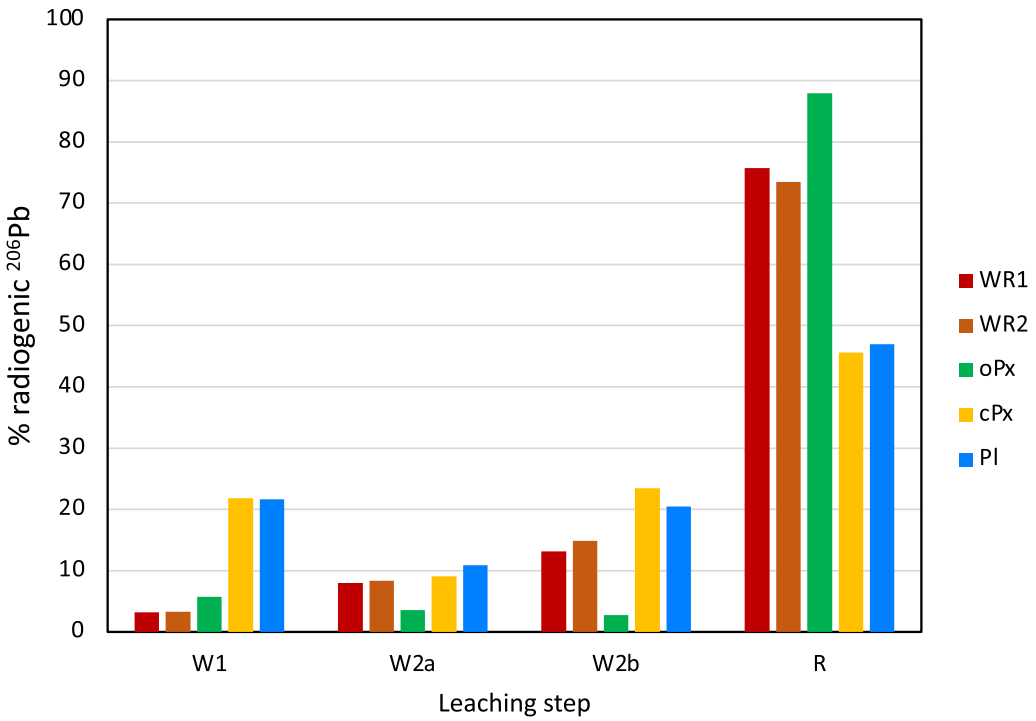

Fig. 2 Distribution of radiogenic ^{206}Pb between leaching steps in whole rock and mineral fractions of ungrouped achondrite Erg Chech 002 (data from batch A167 in Supplementary Data Table 1 of Krestianinov et al. (2023). WR1 and WR2—whole rock fractions, oPx—orthopyroxene, cPx—clinopyroxene, Pl—plagioclase. Leaching steps: W1—0.5 M HNO_3 at ambient temperature with ultrasonication, W2a—hot 7 M HNO_3, W2b—hot 6 M HCl, R—dissolution in hot concentrated HF + HNO_3

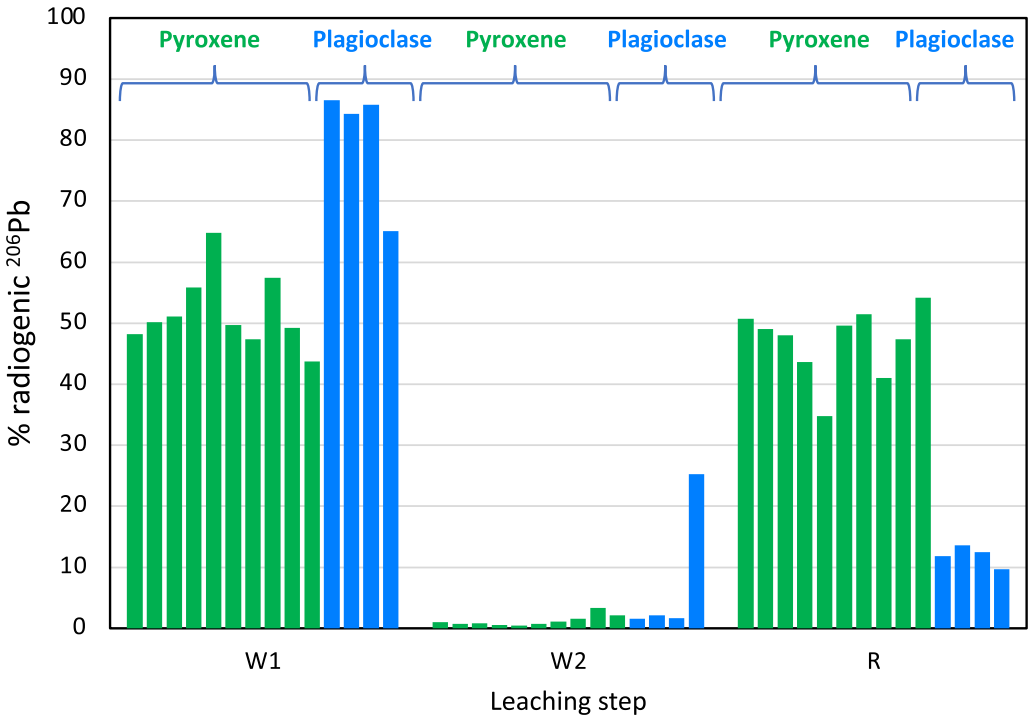

Fig. 3 Distribution of radiogenic ^{206}Pb between leaching steps in whole rock and mineral fractions of ungrouped achondrite Northwest Africa 6704 (Amelin et al. 2019). Green bars—pyroxene, blue bars—plagioclase. Leaching steps: W1—0.5 M HNO_3 at ambient temperature with ultrasonication, W2—combined hot 7 M HNO_3 and hot 6 M HCl, R—dissolution in hot concentrated HF + HNO_3

The loss of radiogenic Pb in modern sample preparation is thus usually small, and the associated expansion of uncertainty is relatively minor. The critical condition of success in using these procedures is their application to materials that are naturally enriched in U and radiogenic Pb, and/or depleted in non-radiogenic Pb, such as zircon and many achondrites and refractory inclusions. If we apply the same procedures in an attempt to date materials that are disturbed by U and Pb migration (e.g., metamict zircon), or contain multiple non-radiogenic Pb components, reliable age determination becomes more difficult and, in some cases, impossible. These difficult cases also require more harsh sample leaching, with associated more extensive loss of radiogenic Pb.

Loss of Pb in mass spectrometry

In thermal ionization mass spectrometry, any analyte, including Pb, can be lost during loading of the sample on the filament, and due to incomplete evaporation from the filament, incomplete ionization, and less than 100% transmission of the mass spectrometer. The first two mechanisms of Pb loss are trivial, and can be avoided by optimizing the procedure. The loss during filament loading can occur if the sample solution contains organics from ion exchange columns, and adheres to the vial and to the pipette tip or capillary tubing that is used for transferring from the vial to the filament. This sticking, and related sample loss, can be prevented by decomposing organics by heating the sample with oxidizing agents such as concentrated HNO_3, aqua regia (an HNO_3–HCl mixture), or hydrogen peroxide.

The loss of Pb due to incomplete evaporation can be avoided by recording the ion beam during the total duration of analysis, from inception of ion emission to complete exhaustion of the sample, in a procedure known as total evaporation TIMS (Callis and Abernathey 1991). In the common current practice of TIMS analysis of sub-nanogram quantities of Pb, the samples are effectively analyzed with total evaporation, either with continuous heating during the run (Amelin and Davis 2006), or by maintaining of a constant intensity by incremental increase of the filament current between blocks. The losses of Pb due to loading problems and incomplete evaporation are thus easily manageable and are minor in well-established analytical procedures.

Processes within a mass spectrometer can significantly reduce the number of Pb ions available for detection. Since the total ion yield determined from mass spectrometer analysis of known quantities of Pb by TIMS is a product of transmission and ionization efficiency, I have to discuss the transmission first in order to evaluate the role of incomplete ionization. Transmission can

be evaluated from total evaporation runs of elements with low first ionization energy, such as alkaline metals Cs (3.89 eV), Rb (4.18 eV), or K (4.34 eV), which ionize in the TIMS source practically quantitatively. The distribution of total evaporation TIMS runs of potassium on a modified MAT 261 mass spectrometer at the Australian National University (Amelin and Merle 2021) is displayed in Fig. 4. The mode of the distribution is ca. 25%, but several runs show total ion yields as high as 50–70%. The total ion yield of 50% has also been reported by Birck (2001) for cesium. From these data, the transmission of well-tuned modern TIMS instruments can be estimated to be 50–70% or higher, and not being among the major causes of Pb ion loss. This estimate probably applies to all TIMS instruments with "extended geometry", designed and built since early 1980s.

The distribution shown on Fig. 4, however, indicates that ion yields achieved in most K analyses are between 20 and 30%, i.e., about half of the maximum values. Variations of the ion yield values in these analyses are most likely related to the small dispersion of filament geometry among the loads, and the related need to compensate the imperfect peak shapes by using lens focus settings that yield adequate peak shapes but lower transmission. These data show the importance of reproducible filament geometry, and keeping the mass spectrometer clean and well-tuned, as well as using the more recent designs of the TIMS source that are less sensitive to variations in the filament geometry, in order to avoid an up to 50% reduction in transmission.

The total ion yield of Pb isotope analysis with the currently universally adopted single-filament, emitter-assisted ionization technique with the best silica gel emitters (Gerstenberger and Haase 1997; Huyskens et al. 2012) reaches ca. 10%. Average values of ion yield in Pb isotope analysis of samples and standards during various studies at the Research School of Earth Sciences, Australian National University, performed on Triton Plus and modified MAT 261 mass spectrometers between 2008–2022 varies between 2.9–4.6% (Fig. 5, and Fig. S2 in Amelin et al. 2010). The difference between maximum and average ion yields in Pb isotope analyses (Fig. 5) is similar to the difference between maximum and average ion yields in K isotope analyses (Fig. 4), and, like the latter, is probably related to the variations in transmission. Considering the contribution of transmission variations, the ionization efficiency of the best available silica gel emitters can be estimated at ca. 10%, i.e., about 90% of Pb is evaporated from the filament in neutral atomic form. Therefore, the uncertainty expansion due to incomplete ionization can be estimated as $1/\sqrt{0.1} \approx 3.2$. The uncertainty expansion due to combined real-life transmission and ionization efficiency, estimated from the average measured ion yields of 4.6–2.9% (Fig. 5 and Amelin et al. 2010), is about 4.7–5.9. This is the most significant source of uncertainty related to Pb loss.

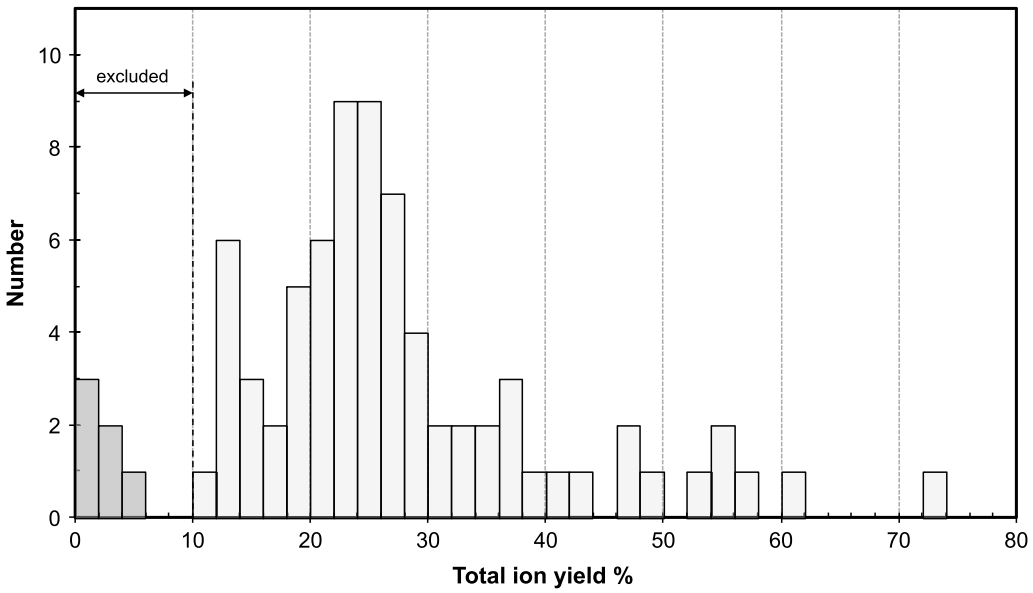

Fig. 4 Total ion yield for potassium in modified MAT 261, from Amelin and Merle (2021). All samples are measured using the total evaporation procedure

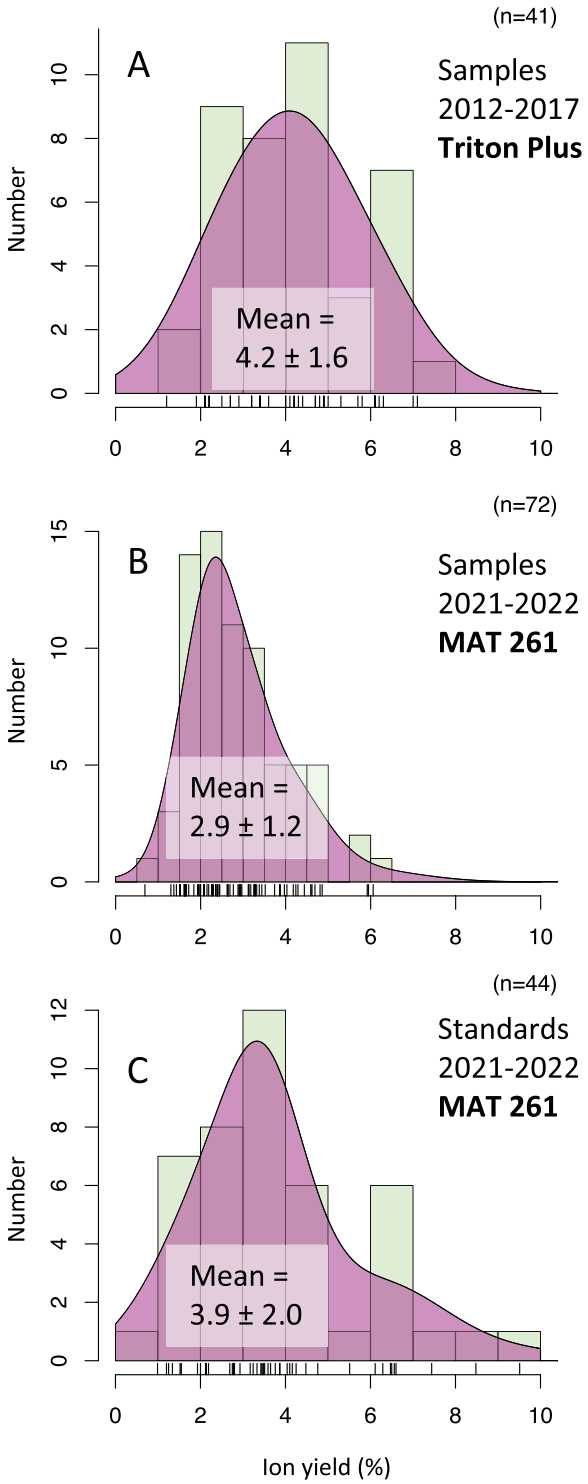

◀ **Fig. 5** Total ion yield in Pb isotope analyses of standards (NIST SRM981 and EarlyTime 1×) and samples at the Research School of Earth Sciences, Australian National University. All samples and standards were loaded with 0.3% Aldrich silica gel emitter (Huyskens et al. 2012). **A** Analyses of rock and mineral fractions of achondrites NWA 6704 and NWA 6693 on Triton Plus between 2012–2017 (data from the table EA4 of Amelin et al. 2019). **B**, **C** Analyses of samples (B) and standards (C) for various projects on modified MAT 261 in 2021–2022

Minimizing analytical noise and bias

In a similar manner to evaluating Pb loss in the previous section, I will go through the steps of the analytical procedure in order to detect the sources of analytical noise and bias. Quantification of additional uncertainties, however, requires a different approach. The relative contribution of the noise components (blank and detector noise) to the total uncertainty depends on the sample size or ion beam intensity and becomes larger as the sample size decreases. The processes that cause analytical biases (leaching-induced fractionation of radiogenic isotopes, and mass-dependent and mass-independent isotopic fractionation in TIMS) introduce systematic uncertainties in the measurements, and correction of these systematic uncertainties is burdened with some random uncertainties. The latter depend on the nature and variability of the bias, and the correction procedure, but generally tend to be independent of the sample size.

Fractionation of radiogenic isotopes of Pb caused by acid leaching

Step leaching in acids that is used for removal of non-radiogenic Pb (section "Loss of Pb* during sample preparation" above) can cause either congruent or incongruent dissolution of minerals. In case of congruent dissolution, all mineral constituent elements go into solution, and elemental ratios in solution are equal to those in the mineral. In case of incongruent dissolution, the mineral structure is broken down such that some elements go into solution, while the other elements remain in the solid phase. In practice of step leaching, it is generally unknown whether mineral dissolution is congruent or not, but commonly observed variations of U/Pb element ratio even in dissolution of single mineral species suggest that dissolution is typically incongruent.

Isotopic fractionation between radiogenic $^{206}Pb^*$ and $^{207}Pb^*$ induced by acid leaching of zircon with substantial radiation damage was described by Davis and Krogh (2000). The possibility that similar fractionation can accompany elemental fractionation in incongruent dissolution of meteorite materials induced by acid leaching was predicted by Amelin et al. (2009), and first observed by Amelin et al. (2010) in a study of Allende Ca-Al rich inclusion (CAI) SJ101, where the effect was caused by a prolonged treatment in hot 9 M HBr. Similar fractionation was subsequently observed in studies of the U–Pb system in achondrite pyroxenes leached with dilute HF (Wimpenny et al. 2019; Amelin et al. 2019). A detailed study of leaching-induced fractionation of the $^{207}Pb^*/^{206}Pb^*$ ratio (Amelin et al. 2024) in achondrites NWA 4801, NWA 10132 and Erg Chech 002 showed that if $^{207}Pb^*/^{206}Pb^*$ fractionation induced by HF leaching goes unnoticed and unchecked, it can produce significant biases of ~ 0.07–0.14% in the $^{207}Pb^*/^{206}Pb^*$ ratios, corresponding to the biases of 1–2 Ma in $^{207}Pb/^{206}Pb$ ages. These biases can thus be about an order of magnitude larger than our target age precision of 0.1 Ma (section "What precision of the isotopic dates do we need?"). These age biases were observed in leaching pairs with highly radiogenic Pb, and cannot be explained by mixing between radiogenic Pb and two non-radiogenic Pb components (primordial, and introduced by terrestrial contamination). The observed isotopic fractionation is thought to be caused by the size difference between α-recoil tracks in the decay chains of ^{238}U and ^{235}U, and by the exsolution of primary pigeonite, leading to the formation of a lamellar structure consisting of augite and low-Ca pyroxene in either post-magmatic or metamorphic reactions. Fortunately, detrimental effect of this fractionation can be reversed by performing a numeric recombination of partial leachate and residue data (Amelin et al. 2024). Currently, it is unclear how pervasive the leaching-induced isotopic fractionation is when considering the practical application of Pb-isotopic chronology to meteoritic materials. It is important to be aware of its effects and to continue to search for an appropriate non-radiogenic Pb removal technique that does not fractionate radiogenic $^{207}Pb^*$ and $^{206}Pb^*$.

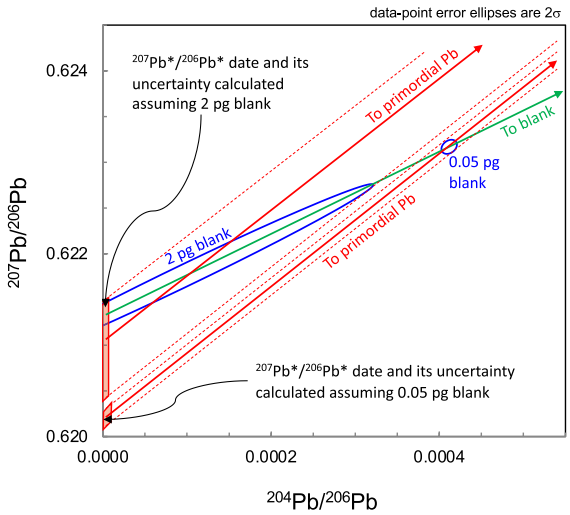

Fig. 6 Schematic presentation of Pb–Pb isotopic data processed assuming low blank and high blank. Small ellipse corresponds to the blank assumed during data reduction: of 0.05 pg with 28% uncertainty, large ellipse—to the blank of 2 pg with the same relative uncertainty. Green arrow shows a mixing line between radiogenic Pb and the blank. Red arrow shows the direction toward primordial Pb, which is assumed to represent initial Pb in the sample. Semi-transparent red vertical bars on the y-axis represent projections of the ellipses from the point of primordial Pb, i.e., the $^{207}Pb^*/^{206}Pb^*$ dates and their uncertainties calculated assuming blanks of 0.05 pg and 2 pg, respectively

Subtraction of analytical blanks

Analytical blanks of procedures used in Pb-isotopic dating show how much extraneous Pb has been introduced to the samples during dissolution, chemical separation, and mass spectrometry. The added extraneous Pb (referred to as blank hereafter) has to be subtracted in order to achieve accurate age calculation. The blank value is burdened with both systematic and random uncertainties, which reflect the accuracy and variability of the blank, and can significantly influence calculated Pb-isotopic ratios and $^{207}Pb^*/^{206}Pb^*$ dates (Fig. 6). Furthermore, accuracy and uncertainty of the blank Pb isotopic composition also influence the calculated dates.

The model for assessment of the effects of blank values on calculated Pb-isotopic ratios and $^{207}Pb^*/^{206}Pb^*$ dates is presented in Additional file 1: Table S1, and its results are plotted in Figs. 7 and 8. The modeling is based on analysis ET1x ZN 110 of the reference material Early-Time 1x, a synthetic isotopic mixture that simulates the radiogenic isotopic composition of Pb at ca. 4560 Ma, and has $^{206}Pb/^{204}Pb$ ratio of ca. 2400. The load containing ca. 88 pg of ^{206}Pb (ca. 200 pg of total Pb), and ca. 23 pg of ^{205}Pb was measured on the modified MAT 261 mass spectrometer in April 2022 using secondary electron multiplier (for $^{206}Pb/^{204}Pb$) and a Faraday cup array with 10^{11} Ω amplifiers (for all isotopes other than ^{204}Pb). The data are reduced using modified AnySpike worksheet of Schmitz and Schoene (2007). Instrumental fractionation was corrected using measured $^{202}Pb/^{205}Pb$ ratio in the spike (Amelin and Davis 2006) and exponential fractionation model. The detailed information about the analysis and parameters used in data processing are shown in the footnote of Additional file 1: Table S1. This analysis represents the best quality of analysis of a small load of

reference material ET1x that could be achieved with the SPIDE^{2}R lab (RSES, ANU) analytical setup.

The following blank parameters are used by default as a reference value for comparisons and are shown with dashed ellipses with increased line thickness. The default blank value of 0.50 ± 0.14 pg (28% RSD), which is typical for processing of meteorite samples at the SPIDE^{2}R lab using the procedures of Amelin et al. (2010, 2019, 2024) in 2021–2022. In analyses of meteorite samples at the SPIDE^{2}R lab the uncertainties of the blank values are estimated by measuring several blanks with each sample batch, and represent the within-batch reproducibility rather than long-term reproducibility. The blank uncertainty of 28% is a typical value for recently measured sample batches. Blank isotope compositions and its RSD uncertainty (^{206}Pb/^{204}Pb = 17.66, 3.1%, ^{207}Pb/^{204}Pb = 15.45, 1.98%) are average values of 123 dissolution and chemistry blanks measured in the batches A142-A186 in 2017–2022 measured alongside meteorite samples at the SPIDE^{2}R lab over the same period of time. Our blank isotope ratios and uncertainties are close to the values reported by the EARTHTIME community: ^{206}Pb/^{204}Pb = 18.41, 2.6%, ^{207}Pb/^{204}Pb = 15.41, 1.88% (Table 5 in McLean et al. 2015). In each of the three sections of the Additional file 1: Table S1 two out three parameters are fixed at the default values, and one is varied as shown in the column B. This approach allows us to evaluate the effect of each of the three parameters separately.

The effect of varying blank value is shown in Figs. 7a and 8a. The uncertainty of ^{207}Pb*/^{206}Pb* date, calculated with zero blank or with zero blank uncertainty, is ± 0.14 Ma, and comprises combined contributions from uncertainty of the fractionation-corrected measured ^{207}Pb/^{206}Pb ratio and uncertainty of the isotopic composition of the spike. The blank-related ^{207}Pb*/^{206}Pb* date uncertainty (red symbols and red line in Fig. 8a) is insignificant for blanks below 0.2 pg, and gradually increases from 0.05 Ma for the default blank value of 0.5 pg, and to 0.27 Ma for a 2.6 pg blank. At the blank of ca. 1.5 pg the contributions to the total uncertainty from the blank subtraction, and from mass spectrometry and spike uncertainties, are equal. At higher blank values, blank subtraction becomes the dominant contributor to the total age uncertainty.

The effect of varying blank uncertainty is shown in Figs. 7b and 8b. In this case, the blank value is fixed at 0.5 pg, and the blank uncertainty is varied from 0 to 2000%. The effect of varying the blank uncertainty on the uncertainty of ^{207}Pb*/^{206}Pb* date is insignificant for blank uncertainty up to 200%. In any reasonably well-established procedure for Pb-isotopic analyses, blank variability does not exceed 50–100%, so this component of the total uncertainty is insignificant.

The influence of the uncertainty of the blank isotopic ratio on the ^{207}Pb*/^{206}Pb* dates is shown in Figs. 7c and 8c. Our estimated uncertainties of blank ^{206}Pb/^{204}Pb and ^{207}Pb/^{204}Pb of ca. 3% and 2%, respectively, contribute additional uncertainty of 0.05 Ma, about three times smaller than the contributions from mass spectrometry and spike subtraction.

Evaluation of the blank subtraction effects presented above, as well as assessments of the blank-related uncertainties in Pb-isotopic data by Connelly et al. (2021) and Gaynor et al. (2022) show that accuracy and isotopic composition of Pb analytical blanks can make significant contribution to the total uncertainty. For the precision of measured, fractionation-corrected ^{207}Pb/^{206}Pb is about 0.003–0.004%, the blank level and uncertainties such as used in the example above are adequate, but further improvements in analytical precision and sensitivity would require blank reduction, and more precise knowledge of its isotopic composition.

A detailed discussion of the strategy of further reduction of blanks and related analytical uncertainties would be beyond the scope of this paper, and here I just outline some general points. It would require identification and ranking of blank components, evaluating the causes of their variability, and checking consistency between the total blanks and the sum of partial blanks. Cleaner ion emitters, better methods of cleaning labware to assure the absence of sample memory and cross-contamination, maintaining dust-free laboratory environment, using the cleanest possible reagents and resins, and refining sample handling procedures are likely to contribute to achieving lower and more consistent blanks.

(See figure on next page.)

Fig. 7 Pb-isotopic data for a reference material EarlyTime 1× (analysis ZN 110) processed with varying blank values (**A**), uncertainties in blank values (**B**), and uncertainties of blank isotopic compositions (**C**). Blank value of 0.50 ± 0.14 pg (28% uncertainty) is typical for Pb procedure that was used for processing of meteorite samples at the SPIDE^{2}R lab, RSES, ANU (Amelin et al. 2010, 2019, 2024). Blank isotope composition and its uncertainty (^{204}Pb/^{206}Pb = 0.05663, 3.1%, ^{207}Pb/^{206}Pb = 0.87882, 0.61%) are the average values measured alongside meteorite samples at the SPIDE^{2}R lab in 2021–2022. These blank parameters are used a reference value for comparisons, and are shown with dashed ellipses with increased lime thickness. The blank values (pane **A**) are from 0 to 2 pg with 28% uncertainty. Blank uncertainty values (pane **B**) are between 0 and 100% and are applied to 0.5 pg blank. Uncertainties of blank isotopic composition are calculated by multiplying the uncertainty reference values (3.1% for ^{204}Pb/^{206}Pb and 0.61% for ^{207}Pb/^{206}Pb) by factors between 0.1 and 20. Further details can be found in the Additional file 1: Table S1

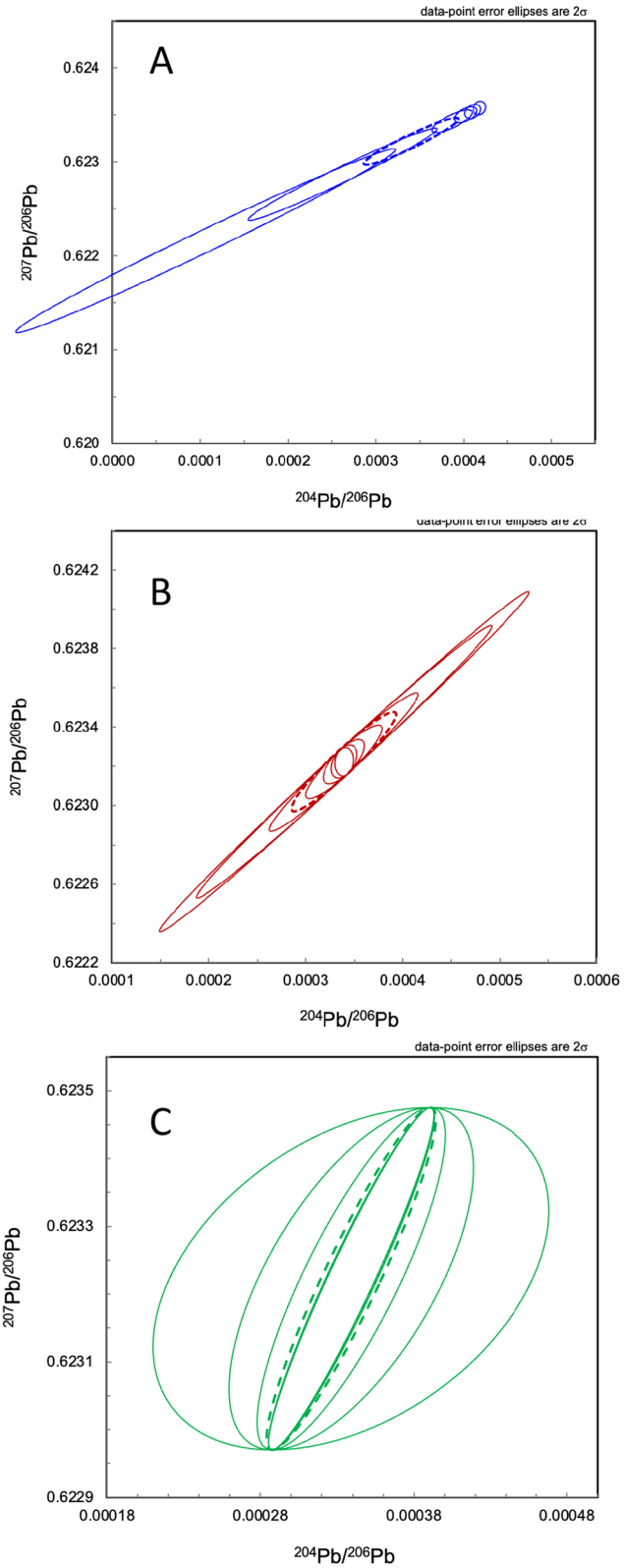

Fig. 7 (See legend on previous page.)

A separate, although related, topic is the isobaric interferences in Pb isotope analyses, most importantly on the low-abundance isotopes, which can compromise determination of the blanks and their variability, as well as the measurement of ^{204}Pb in the samples. These interferences are likely to have masses that are slightly different from the masses of Pb isotopes, but cannot be completely resolved due to low mass resolution (around 400) of TIMS instruments. However, the volatility of the interfering species is likely to be different from volatility of Pb. Therefore, the absence of interferences can be verified by measuring the samples (and reference materials and blanks) over sufficiently broad range of temperatures, and assuring that the ratios of the least abundant isotope ^{204}Pb to more abundant (and hence less interference-prone) isotopes remain constant. Such a measurement procedure would be well aligned with the total evaporation approach that is used to maximize the total ion yield (section "Loss of Pb in mass spectrometry" above).

Correction of mass-dependent fractionation

Another source of uncertainty introduced by Pb isotope analysis in TIMS is fractionation of isotopes during evaporation from the filament. The largest fractionation component is mass-dependent. Its magnitude is on the order of 0.1–0.2% per atomic mass unit (amu), which is ca. 15–30 times larger than the significance threshold of 0.007% adopted in this study. Furthermore, the isotopic composition of Pb that is evaporated from the filament gradually shifts toward heavier isotopic composition due to preferential evaporation of lighter isotopes.

The effect of isotopic fractionation in TIMS can be corrected by external or internal "normalization" of all measured isotopic ratios to the known value of one isotopic ratio. External normalization is performed by measuring reference materials with known isotopic composition, and applying average fractionation values to analyses of samples. For Pb, this method has uncertainty of ca. 0.03–0.05% per amu, which is ca. 4–7 times larger than our significance threshold. In addition, this method provides accurate correction only if analytical conditions, including presence of organics and residual matrix elements from sample preparation, are identical for reference materials and unknowns. This poses a problem when we use pure salts of Pb as reference materials to correct fractionation in analyses of Pb chemically separated from rocks and minerals. External fractionation correction thus cannot be considered satisfactory when we aim to achieve precision of the ^{207}Pb/^{206}Pb ratios ca. 0.007% or better.

Using double spike (Dodson 1963) provides more precise and accurate isotopic fractionation correction, including compensation of changing of measured isotopic compositions during analysis, similar to "internal" normalization in isotope analysis of elements (e.g., Sr and Nd) that have at least one isotopic ratio that can be considered invariable. In the "classical" version of double spiking (Compston and Oversby 1969), Pb separated from the sample is split into two aliquots, one of which is spiked with a mixture of two natural Pb isotopes, most commonly ^{207}Pb and ^{204}Pb, before loading on the filament, while the other is measured unspiked. In the alternative version (Todt et al. 1996), a spike made of two artificial isotopes ^{202}Pb and ^{205}Pb is added to the sample before dissolution and chemical separation, thereby enabling direct internal normalization. This approach requires only one mass spectrometer run, from which precise fractionation-corrected Pb isotopic composition as well as Pb concentration are calculated.

The advantages of the ^{202}Pb-^{205}Pb double spike compared to ^{207}Pb-^{204}Pb and other "natural isotope" double spikes in efficiency, simplicity of use, and most importantly, the absence of risk that an unspiked aliquot gets accidentally contaminated with ^{207}Pb and ^{204}Pb, make this spike a clear choice for Pb-isotopic and U–Pb analyses. Modern implementations of this spike (Amelin and Davis 2006; Condon et al. 2015) brought about the current precision level of Pb isotope analysis in 10^{-11}–10^{-9}-g quantities, and provide a firm background for improvement of the other aspects of Pb isotope analytical

(See figure on next page.)

Fig. 8 Uncertainty of the ^{207}Pb*/^{206}Pb* model dates for the reference material EarlyTime 1 × calculated from the data processed with varying blank parameters: blank value, blank uncertainty, and uncertainty of the blank isotopic composition. The data processing parameters are described in the caption of Fig. 7. The data are calculated using the uncertainties of the measured isotopic ratios and uncertainties of the spike isotopic compositions as shown in the footnote of the Additional file 1: Table S1. Model dates and their uncertainties are calculated from two-point ^{207}Pb/^{206}Pb versus ^{204}Pb/^{206}Pb isochrons that include primordial Pb as the second point (initial isotopic composition), regressed in IsoplotR (Vermeesch 2018) using the default maximum likelihood model. The data points corresponding to default values of the blank parameters are encircled. Blue and red lines show total uncertainties and blank-related uncertainty components, respectively. Horizontal black dashed line shows the level of uncertainty from measured isotopic ratios and spike isotopic compositions at zero blank. **A** Uncertainty of the ^{207}Pb*/^{206}Pb* model date versus blank value (picograms). **B** Uncertainty of the ^{207}Pb*/^{206}Pb* model date versus relative uncertainty (%) of the blank. **C** Uncertainty of the ^{207}Pb*/^{206}Pb* model date versus uncertainty of the blank isotopic composition, expressed as a multiplier to the accepted value of the Pb blank uncertainty at RSES ANU in 2020–2022

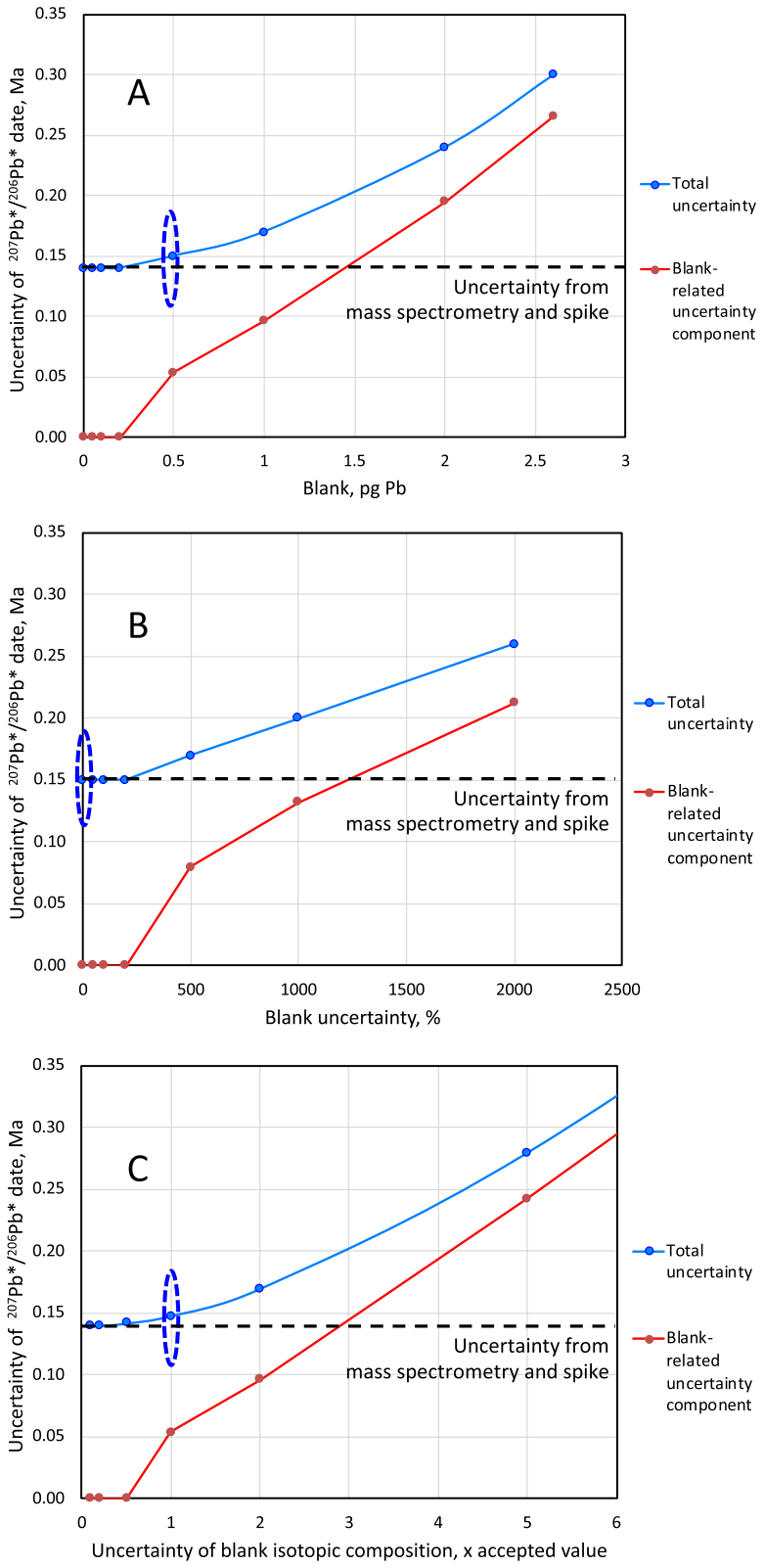

Fig. 8 (See legend on previous page.)

techniques. Unfortunately, the availability of the ^{202}Pb-^{205}Pb double spike and its components is limited, and this could pose the problem in the future as the current stocks are running out.

A potential problem with the normalization procedure is that isotopic fractionation of elements during evaporation can follow various patterns or "laws" (e.g., Russell et al. 1978; Hart and Zindler 1989; Davis et al. 2015). This is an important technical issue in isotope analyses where precision at the part per million level is required. However, it is likely to be less of a problem for Pb. The differences between isotopic ratios for light elements such as Mg and Ca corrected for fractionation using different fractionation "laws" (excluding the internally inconsistent and largely abandoned "linear law") are less than 5% of the overall magnitude of fractionation. If the same relationship holds for Pb, we can expect the additional uncertainty due to the choice of fractionation "law" to be around 0.01% in the worst case, and commonly much lower, and hence below our significance threshold. It would be highly desirable to explore the pattern of mass-dependent fractionation of Pb during evaporation from silica gel in the future, as the total uncertainties of analyses get lower.

Spike subtraction

In addition to the main isotopes ^{202}Pb and ^{205}Pb, double spikes that are used for calculating Pb concentration and correction of isotope fractionation contain small amounts of ^{204}Pb, ^{206}Pb, ^{207}Pb and ^{208}Pb. For accurate calculation of natural ^{204}Pb/^{206}Pb and ^{207}Pb/^{206}Pb ratios, the quantities of ^{204}Pb, ^{206}Pb and ^{207}Pb derived from the spike have to be subtracted from the total measured quantities of these isotopes, in a manner similar to the blank subtraction. The uncertainty in the ^{207}Pb/^{206}Pb ratio introduced by spike subtraction depends on the abundance of minor isotopes, uncertainty of their abundance, and the sample / spike mixing ratio.

The abundance of minor isotopes is defined by the preparation of enriched ^{202}Pb and ^{205}Pb. In the currently used ^{202}Pb-^{205}Pb spikes and their components (Wasserburg et al. 1977; Todt et al. 1996; Amelin and Davis 2006; Condon et al. 2015; McLean et al. 2015; Huyskens et al. 2016), the ratios of minor Pb isotopes to ^{205}Pb (or ^{202}Pb) are mostly between 10^{-4} and 10^{-3}, with the exception of elevated abundance of ^{206}Pb in the ^{205}Pb spike prepared by proton irradiation of ^{206}Pb with subsequent decay of ^{205}Bi to ^{205}Pb (Parrish and Krogh 1987). Considering limited availability of these spikes, the researchers who use the spike have no control over the abundances of minor isotopes, unless they undertake an ab initio preparation of ^{202}Pb and ^{205}Pb.

While the abundances of minor Pb isotopes ^{202}Pb-^{205}Pb spikes cannot be easily reduced, they can be measured more precisely, and this would facilitate more precise and accurate spike subtraction. Precise determination of the minor Pb isotope abundances is, however, complicated by the contribution from loading blanks, which is greatly amplified by the large difference in isotope composition between the spike and the blank. Blank-corrected spike isotopic composition can be determined from spike-blank mixing lines, constructed by running various quantities of the spike, as described in detail by McLean et al. (2015) and Huyskens et al. (2016). The 2σ uncertainties of the ratios between minor isotopes of Pb and ^{205}Pb are around 10–20% (Condon et al. 2015; Huyskens et al. 2016).

Mixing ratio between the sample and spike Pb varies between samples, and is within control of the analyst. The optimal mixing ratio is a trade-off between having sufficient number of ^{202}Pb and ^{205}Pb for precise measurement of the ^{202}Pb/^{205}Pb ratio and calculating precise fractionation correction, and keeping the uncertainty of spike subtraction sufficiently low. The dependence of uncertainty in the ^{207}Pb*/^{206}Pb* date on the sample-spike mixing ratio (expressed by measured ^{206}Pb/^{205}Pb ratio) is shown in Fig. 9 for uncertainties of the spike ^{204}Pb/^{205}Pb, ^{206}Pb/^{205}Pb, ^{207}Pb/^{205}Pb and ^{208}Pb/^{205}Pb ratios of 10%, 20% and 30%. For ^{206}Pb/^{205}Pb ≥ 1 and uncertainties of spike minor isotope abundances of 10–20%, the typical current precision level, the contribution to the ^{207}Pb*/^{206}Pb* date uncertainty from spike subtraction is below the accepted significance threshold of 0.1 Ma, and becomes insignificant at higher sample to spike ratios. On the other hand, for overspiked samples the subtraction of spike can be a significant, and possibly dominant, component of the total date uncertainty, especially if the spike isotopic composition is less precisely known. It should be noted that Fig. 9 gives only a crude evaluation of the spike subtraction uncertainty, because it does not account for possible error correlations between individual ratios of minor isotopes in the spike. Nevertheless, it clearly shows that the currently available ^{202}Pb-^{205}Pb spiked can be used to measure ^{207}Pb*/^{206}Pb* ratios without significant additional uncertainty if their isotopic compositions are more precisely measured, and the ^{206}Pb/^{205}Pb ratios above 1 are maintained.

Mass-independent isotopic fractionation

Isotope fractionation is TIMS can include a mass-independent component in addition to the main mass-dependent fractionation. For Pb, it was first observed as a systematic downward shift of the ^{207}Pb/^{206}Pb isotopic ratio normalized to ^{208}Pb/^{206}Pb toward the end of

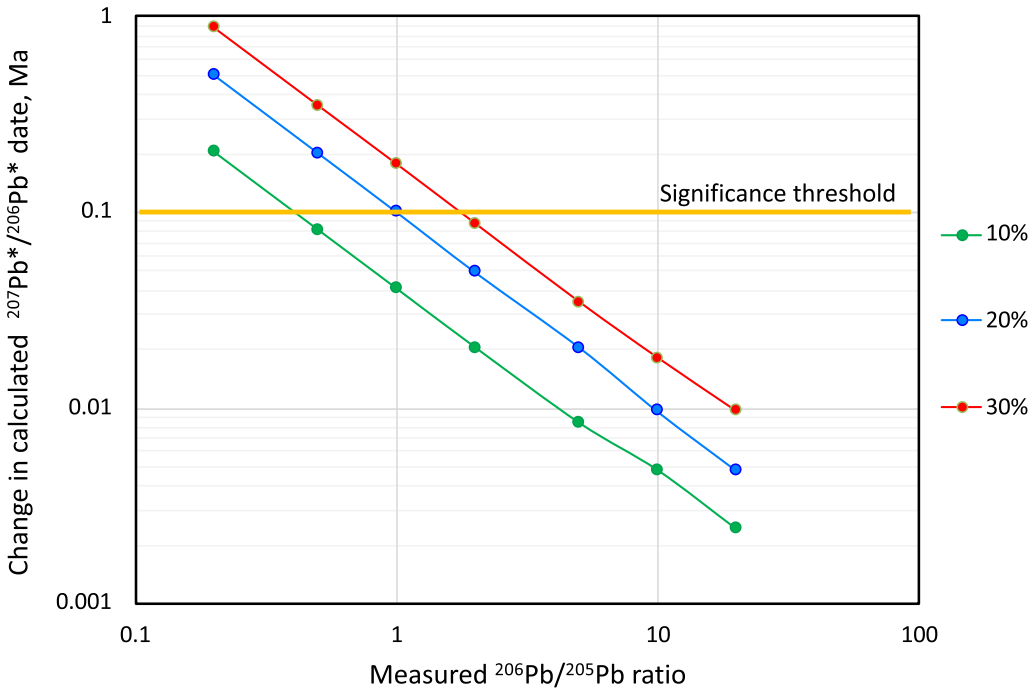

Fig. 9 Changes in the $^{207}Pb^*/^{206}Pb^*$ model dates for the reference material EarlyTime 1× (the same analysis as shown in Figs. 7 and 8) as a function sample/spike ratio, expressed as fractionation-corrected $^{206}Pb/^{205}Pb$ ratio. Green, blue and red lines represent 10, 20 and 30% changes, respectively, in the abundances of minor isotopes in the ^{202}Pb-^{205}Pb spike, expressed as the ratios of ^{204}Pb, ^{206}Pb, ^{207}Pb and ^{208}Pb to the major isotope ^{205}Pb, assumed in the data reduction. The horizontal orange line shows the significance threshold adopted in this study

analysis (Thirlwall 2000; Doucelance and Manhès, 2001). Analyses of mixtures of reference material SRM 981 containing four natural isotopes of Pb and ^{202}Pb-^{205}Pb spike (Amelin et al. 2005b) have shown that the deviation from mass-dependent fractionation pattern is not unique for ^{207}Pb, but can be approximately described as decoupling of fractionation of odd-mass isotopes ^{205}Pb and ^{207}Pb from fractionation of even-mass isotopes ^{202}Pb, ^{204}Pb, ^{206}Pb and ^{208}Pb. Since the $^{207}Pb/^{206}Pb$ ratio includes an even-mass and an odd-mass isotope, and the magnitudes of mass-dependent and mass-independent fractionation are only broadly correlated, the effects of anomalous fractionation cannot be completely eliminated by internal normalization. It has been suggested (Amelin et al. 2005b) that this fractionation component is related to nuclear field shift (Bigeleisen 1996), although the details of its nature and mechanism remain unclear.

The magnitude of odd–even isotope fractionation of Pb depends on the chemical formulation of the silica gel emitter and increases as the sample evaporation progresses. The existing TIMS data (Amelin et al. 2005b) suggest that mass-independent fractionation of $^{207}Pb/^{206}Pb$ ratio for Pb loaded with the Merck silicic acid emitter of Gerstenberger and Haase (1997), the most popular ion emitter in TIMS Pb isotope analyses, can be kept below 0.01%, and in most cases below 0.005%, by limiting the extent of sample evaporation to 60–70%. The mass-independent fractionation of Pb can be therefore maintained close to, or below, our significance threshold, if we can tolerate a moderate reduction of the total ion yield due to excluding the data collected at the end of analysis. With increase of analytical precision that can be expected in the future, mass-independent fractionation of Pb can become a significant contributor to the total uncertainty, and it would be necessary to develop the methods for minimizing or correcting this effect.

Noise, losses and biases related to the ion detection system

The design and way of operation of ion detection systems influence precision and accuracy of measured isotopic ratios in a complicated way (Carlson 2014). The efficiency of ion detection can be close to 100%, or about an order of magnitude lower. The added noise can be high, or practically absent. The introduced biases that cause systematic uncertainties in the measured ratios vary from negligible to significant. Unfortunately, no existing system for ion detection combines the advantages of high efficiency, low noise and the absence of biases. The design of ion detectors, and developing an optimal way of their usage, is always a search for a compromise that is less detrimental to precision and

accuracy of the isotopic ratios. Because of the complex interplay between noise, losses and biases that originate from the ion detection systems, these topics are discussed together in a dedicated section.

This discussion is restricted to "conventional" systems based on Faraday cups connected to various types of electrometer amplifiers, and ion counting systems, such as used in modern TIMS (and multicollector ICPMS) instruments. Other detectors that are used in different types of mass spectrometers are not considered here.

Duty cycle of single collector and multicollector ion detection

The loss of ions in the detection system can be described in terms of duty cycle—a fraction of one measurement period in which a signal is being registered. Let us consider isotope analysis of Pb with ^{202}Pb-^{205}Pb spike, and monitoring interferences at masses 201 (^{138}Ba^{31}P^{16}O$_2$) and 203 (^{203}Tl). If we use a mass spectrometer with 8 or more detectors that can be positioned for simultaneous detection of ions beams at all masses between 201 and 208, and with sufficiently high baseline stability to allow measurement of the baseline before the beginning of ion beam acquisition, then the duty cycle of ion detection is approaching 100% for all measured isotopes. A small fraction of time required for centering and focusing of ion beam is typically between 2–10%, and reduces the effective analysis duty cycle to 90–98%. If, instead we are using a mass spectrometer with a single collector to measure the same peaks, and set the integration time for each peak at the same value (e.g., 4 s) and the idle time between the peaks to allow magnet field settle at half that time (2 s), then the duty cycle of for each isotope will be mere 8.3%, or even lower if we consider time for centering and focusing. In this example, the multicollector system has a 12 times advantage in duty cycle, and hence in counting statistics, which translates into ca. 3.5 times advantage in precision based on the equations in section "Relationship between precision of isotopic ratios, sample size, and performance of the analytical procedure". Increasing integration time, decreasing idle time, re-arranging integration time between isotopes, and skipping less important interference corrections can improve duty cycle of single collector measurements, but only slightly. Furthermore, these measures are associated with additional downsides and potential problems, e.g., making the measurements more sensitive to ion beam instability, and increasing the risk of undetected interferences. The advantages in efficiency of simultaneous detection with a multicollector system thus are clear and obvious. Simultaneous detection also has an advantage of making measurements practically insensitive to the relatively slow ion beam variations that are observed in TIMS.

Multicollector arrays can be constructed using either Faraday cups with electrometers, or ion counting multipliers, or their combination. All modern TIMS instruments are equipped with Faraday multicollector arrays containing up to 9–16 channels—a sufficient number for Pb isotope analysis in static mode. Daly detectors and regular size secondary electron multipliers are larger than Faraday cups, and fitting similar number of these detectors in mass spectrometers is not possible without increasing instrument dispersion and hence magnet size, which would make the instrument much larger and more expensive. One possible solution is to use smaller ion counters—continuous dynode multipliers (channeltrons) or compact discrete-dynode multipliers (CDDs). These ion counters have, however, their own set of problems: poor peak shape, and often limited dynamic range and poor linearity. The other solution is to design a system with a smaller number of regular-size ion counters of the best available quality. Such systems include up to 5 secondary electron multipliers and/or Daly detectors. Isotope analysis of Pb with ^{202}Pb-^{205}Pb spike using such detector system would require 2–3 mass steps to cover the required mass range. The duty cycle of such analyses for Pb isotopes most demanding for precision (^{202}Pb, ^{205}Pb, ^{206}Pb and ^{207}Pb) can be up to 40–80%, so the reduction of precision due to ion loss would be moderate (up to ca. 1.5 times). If an array of high-quality ion counters can be made to operate with acceptable level of systematic uncertainties, then it can be an attractive option for Pb isotope analysis with minimum ion loss.

Noise of ion detection systems

Faraday cup multicollector systems have been installed in both commercial and custom-built mass spectrometers (e.g., Esat 1984) since early 1980s, but, despite their obvious advantages, single collector ion counting remains the preferred ion detection system for Pb-isotope analysis in ID-TIMS U–Pb geochronology (Schoene 2014; Schaltegger et al. 2021), and is successfully used in Pb-isotope dating of meteorites (e.g., Connelly et al. 2012). The reason for sustained popularity of ion counters is their excellent noise characteristics. Dark noise of secondary electron multipliers, and photomultipliers that are used in Daly detectors, is typically around 0.02–0.1 counts per second (cps), or 0.32–1.6*10^{-20} A, which is 2–3 orders of magnitude lower than the typical ion beam of the least abundant isotope ^{204}Pb in the samples with the lowest content of common Pb. The contribution of this noise to the measurements of more abundant Pb isotopes is completely negligible.

On the other hand, the noise of electrometer amplifiers (Low level measurements handbook 2004) connected to Faraday cups, is substantial. In most common

electrometers that include a high-value resistor in the feedback circuit, the main component of the total amplifier noise is thermal or Johnson–Nyquist noise (Johnson 1928; Nyquist 1928). The magnitude of resistor thermal noise, expressed in current or voltage units, is

$$I = \sqrt{(4 * k * T * \Delta f / R)} \quad (12)$$

$$V = \sqrt{(4 * k * T * \Delta f * R)} \quad (13)$$

where I is the noise current, V is the noise voltage, k is Boltzmann constant, T is absolute temperature, R is feedback resistance, and Δf is frequency—a reciprocal value of the integration time (Ireland et al. 2014).

The values of resistor thermal noise (Additional file 1: Table S2) strongly depend on frequency. The temperature dependence of the noise near ambient temperature is, however, rather small: increasing the temperature from 16 °C (such as Phoenix and Isoprobe T at KBSI) to 38 °C (as in Triton Plus at ANU) changes the thermal noise by 3.7%. There is, therefore, almost no inherent difference in noise between mass spectrometer designs that use heating or cooling to stabilize temperature of electrometer assembly, and hence gain ratios between channels.

Thermal noise changes proportionally to the square root of the feedback resistance, while the output voltage changes proportionally to the feedback resistance, therefore an electrometer with higher feedback resistance allows us to measure ion beams with higher signal to noise ratio. If thermal noise was the only (or by far the dominant) component in the total amplifier noise, then the noise advantage would be proportional to the square root of the feedback resistance, i.e., an amplifier with 10^{12} Ohm feedback resistor would give 3.16 times higher signal to noise ratio than an amplifier with commonly used 10^{11} Ohm feedback resistor, whereas an amplifier with 10^{13} Ohm feedback resistor would give 10 times higher signal to noise ratio than an amplifier with 10^{11} Ohm feedback resistor. The presence of other sources of noise that do not scale with feedback resistance (e.g., Ireland et al. 2014) makes the real-life noise advantage of very high-Ohm amplifiers smaller, but it is still significant and provides a substantial advantage in precision of measurements of small ion beams (Koornneef et al. 2014). Mass spectrometers equipped with electrometers with 10^{13} Ohm amplifiers are now successfully used in Pb-isotope analysis in U–Pb ID-TIMS geochronology (e.g., von Quadt et al. 2016; Zhou et al. 2019).

Using electrometers with capacitors in the feedback circuit to measure ion beams in charge mode (Esat 1995; Ireland et al. 2014) makes it possible to avoid Johnson–Nyquist noise altogether. Measurements in charge mode are burdened with thermal noise of the capacitor (Esat 1995):

$$V = \sqrt{(k * T / C)} \quad (14)$$

where C is capacitance, and the other symbols are the same as for Eqs. 12 and 13. This noise reflects statistical equilibrium of the charge in the capacitor, and is apparent only for the reading of the capacitor (Ireland et al. 2014). Therefore, the contribution of the capacitor thermal noise can be reduced by longer integration time and less frequent capacitor reading. The charge mode has been recently implemented in ATONA amplifiers that are installed in TIMS (and noble gas) instruments manufactured by IsotopX. Using an array of ATONA amplifiers for Pb and U isotope analysis has yielded better precision than measurements with a single Daly ion counter for the signals larger than $0.5–1 \times 10^{-14}$ A, which can be achieved for major isotopes of Pb for ca. 10 pg and larger loads (Szymanowski and Schoene 2020).

A charge collection amplifier of the next generation called Zeptona (Hockley et al. 2021) is claimed by the manufacturer to yield an order of magnitude reduction of current noise compared to the ATONA systems, and is offered as an upgrade to the latter. To the best of my knowledge, there are no data from user laboratories showing the Zeptona performance so far. A notable feature of this design is that the Zeptona amplifier must be connected to a dedicated fixed Faraday cup. This suggests that flexible wiring and/or other elements of movable Faraday cup assembly of current generation can be a source of noise comparable in magnitude to the noise of the best electrometer amplifiers.

The difference between the thermal noise of feedback resistors and the dark noise of ion counters is huge. Even if we use conservative estimate of the dark noise of 0.1 cps (which is typically observed when multipliers approach the end of their usable lifespan), the thermal noise of an amplifier with 10^{13} Ohm feedback resistor is ca. 2,500 times higher than the multiplier dark noise, and the thermal noise of an amplifier with 10^{11} Ohm feedback resistor is ca. 25,000 times higher.

Long-term stability of amplifier electronic baselines

In addition to noise, which is getting lower with increasing integration time, electrometers can exhibit longer-term changes in the readings of electronic baselines (which are referred to simply as baselines hereafter). Long-term stability of the amplifier baseline dictates the strategy of baseline measurements, which in turn influences duty cycle. If the amplifier is free from detectable drift or fluctuations at the scale of tens of minutes, or hours, then the baseline can be measured during sample warm-up, and all time of good quality ion emission can be used to acquire ion beam. If the baseline is

drifting and/or fluctuating, it has to be measured more frequently, thereby reducing duty cycle.

A summary of amplifier noise measurements is shown in Additional file 1: Table S3 for three TIMS instruments: Triton Plus at the ANU and Isoprobe T at KBSI with 10^{11} Ohm amplifiers operated in current mode, and Phoenix at Guangzhou Institute of Geochemistry with ATONA amplifiers operated in charge mode. The measurements were run for 1.4–3.0 h, and one extra-long measurement was run for 36 h. Comparison of the ratios of measured to theoretical (Johnson–Nyquist) noise at different integration times reveals both noise and drift patterns of the amplifiers. For the purpose of this discussion, this ratio is called normalized noise. In an instrument with electrometers where Johnson–Nyquist noise is the main noise component, and long-term drift and fluctuations are absent, the normalized noise is close to unity irrespective of integration time.

For both instruments with amplifiers in current mode, short-term (5–8 s) normalized noise is close to unity. In the Triton, the normalized noise increases only slightly (up to ca. 1.4×) for ca. 80–800 s integration, but increases very significantly (6.6×) for the 36-h run. In the Isoprobe T, the normalized noise is close to 1 for 5 s integrations, but increases significantly (3.1×) for 500 s integrations. These data show that the Triton amplifiers are drifting at the scale of several hours, but are practically free from drift/fluctuations at the scale of minutes. In contrast, the Isoprobe T amplifiers are already drifting or fluctuating significantly at the scale of several minutes. Isotopic analyses with both of these instruments thus require frequent baseline measurements, but the drift problem is more serious in the Isoprobe T.

Baseline measurements of ATONA amplifiers in the Phoenix reveal a different pattern: normalized noise is steadily reduced with increasing integration time. The data for this instrument indicate the absence of measurable baseline drift or fluctuations over 1.4–2.8 h. Reduction of the normalized noise for longer integrations is probably related to smaller contribution of the capacitor reading noise. An optimal measurement strategy with this instrument would be to measure the baselines during sample warm-up and use the longest possible measurement intervals between amplifier readings for ion beam acquisition.

Dynamic range of the ion detection systems

The upper limit of the ion beam current that can be measured with electrometers with 10^{11} Ohm resistors, and charge amplifiers that are installed in modern TIMS, is between 10^{-9} and 10^{-10} A, and does not pose any restriction for isotope analyses of sub-nanogram to low nanogram quantities of Pb, where the ion beams rarely exceed 10^{-11} A and are typically much smaller. As the resistivity of the feedback resistors of electrometer amplifiers increase, the upper limit of measurable current is reduced proportionally. For example, the amplifiers installed in Tritons have maximum measurable current of 5×10^{-10} A with 10^{11} Ohm resistors, and 5×10^{-12} A with 10^{13} Ohm resistors. Still, even with 10^{13} Ohm amplifiers the upper limit of the measurable current is rarely a problem in Pb isotope analyses in geochronology.

The situation is different for ion counters. Continuous dynode multipliers often have the upper limit of the counting rate of ca. 10^5 cps, i.e., 1.6×10^{-14} A. This is too low for measuring all samples in modern U–Pb dating, with possible exception of the very smallest loads with reduced amount of ^{202}Pb-^{205}Pb spike. Discrete-dynode multipliers allow counting rates up to $1–1.5\times10^6$ cps ($1.6–2.4\times10^{-13}$ A), and Daly detectors—up to 3×10^6 cps (ca. 5×10^{-13} A). These current limits are adequate for most Pb loads analyzed in U–Pb geochronology, but the measuring conditions for samples containing more than 100–200 pg of Pb can be less than optimal.

Accuracy of the ion detection systems

Accuracy of ion detection systems is a multifaceted problem. In includes linearity of individual detectors, stability of relative efficiencies of detectors used together for static multicollector ion beam acquisition, and the difficulty of precise cross-calibration of multiple detectors. Modern electrometer amplifiers are designed for achieving precision and accuracy of linearity and relative gain stability at part per million level, as illustrated, for example, by gain reproducibility (RSD) of 0.0002–0.0004% in the ANU Triton Plus over one month in 2021. The amplifiers in multicollector systems are precisely and accurately cross-calibrated by applying the same current from a stable current source to each amplifier. The influence of these parameters on Pb isotope analysis at our significance level of 0.007% can be safely considered negligible.

Faraday cups can be affected by imperfect efficiency—a partial loss of charge due to emission of secondary electrons or ions or both. Cup efficiency usually shows long-term drift caused by deposition build-up inside Faraday cups, and related changes of their emission properties (Holmden and Bélanger 2010). Non-unity cup efficiency can be corrected for (Davis 2020; Di et al. 2021, and references therein) and can be reset to unity by replacing or cleaning cup liners. In any case, the deviation of cup efficiency from unity rarely reaches our significance threshold of 0.007% and usually is not considered a problem in geochronological Pb isotope analyses.

Nonlinearity of ion counters is generally much greater than nonlinearity of electrometer amplifiers. The component of ion counter nonlinearity that depends on their design has been a substantial problem in the past (Richter et al. 2001), but has been greatly reduced in the modern design of both secondary electron multipliers and Daly systems (e.g., Palacz et al. 2011). Another nonlinearity component, caused by a period of non-responsiveness during processing of a pulse (called dead time) is inherent to ion counting. In all modern ion counting detectors dead time (usually in the order of tens of nanoseconds) is measured, and appropriate corrections are applied. Two factors limit, however, the effectiveness of these corrections. Firstly, the dead time measurement has its own uncertainty, which contributes to the uncertainty of the measured counting rate of the ion beam. Secondly, the magnitude of correction increases with the ion beam intensity, and eventually nonlinear components, related to arrival of two or more ions during the period of non-responsiveness, are becoming significant. Uncertainty and nonlinearity of dead time correction are among the main reasons why the upper limits of operation of ion counters are restricted at $1–3 \times 10^6$ cps.

Multicollector systems composed of ion counters cannot be cross-calibrated by applying constant current, as it is done with electrometer amplifiers. Instead, these systems are calibrated by measuring a stable ion beam sequentially with each ion counting channel. This procedure takes several hours, and requires very stable ion beam of optimal intensity (high enough to achieve good counting statistics, but below the operating maximum), but can be done with uncertainty of 0.002–0.003%, well below our significance threshold. The problem is, however, that the relative gains of amplifiers tend to drift. In a study of performance of Pb multi-ion counting array (consisting of three regular size MasCom MC TE-Z/17 multipliers and two CDD multipliers) in the ANU Triton Plus TIMS, Amelin and Huyskens (2013) determined the drift of relative gains by 0.05–01% per hour.

An alternative way of using the multiplier array is to measure signal at several mass steps, treat each channel as an individual detector, and pool the measured isotopic ratios. This approach does not depend on the multiplier gain stability, and can potentially produce precise and accurate results. However, it requires either peak flatness at the level of ca. 0.01% over the range of peak misalignment between mass steps, or changing the dispersion quadrupole settings between the mass steps to keep the peaks aligned (if the instrument is equipped with a zoom lens to change dispersion), to circumvent the effects of imperfect peak flatness, which in the case CDD multipliers can exceed 1%. The tests by Amelin and Huyskens (2013) on the ANU Triton plus showed that setting the dispersion quadrupole to ± 10 V changes the SEM gains by 0.1–0.3%, and to ± 20 V by up to 1.2%. The changes of the dispersion quadrupole settings required to keep the peaks aligned in the five-step multicollector procedure that was necessary to cover the mass range from 201 to 208 were up to 16, which causes a ca. 0.6–0.8% changes in SEM gains. Such changes of SEM gains between the mass steps are unacceptably large for U–Pb geochronology. No similar effect is observed for Faraday cups down to 0.002% precision level.

These tests indicate that the Pb multi-ion counting array in the instruments like the ANU Triton Plus is adequate for measurements at ca. 0.1% level of precision and accuracy, as long as the dispersion setting is unchanged. Achieving a precision level close to our significance threshold for the needs of modern U–Pb geochronology would require either radical improvement in the multiplier gain stability, or a more thorough understanding of the interplay between the zoom optics and the multipliers. Similar tests of multicollector ion counting systems in other types of TIMS would be highly desirable.

Theoretical uncertainties for ancient radiogenic Pb and their dependence on the measurement conditions

Using measured baseline noise characteristics presented in Additional file 1: Table S3, we can calculate uncertainties for isotope analysis of Pb with atomic abundances of $^{206}Pb = 25\%$ and $^{207}Pb = 15.5\%$ (corresponding to $^{207}Pb/^{206}Pb = 0.62$, a radiogenic isotope composition for a 4555 Ma material). The calculations are presented in Additional file 1: Table S4, and their results are shown in Figs. 10 and 11. In the absence of noise (black lines in Figs. 10 and 11), the minimum sample size required to achieve analytical precision corresponding to significance threshold of 0.007% in static multicollector measurements (100% duty cycle) is 2.9 pg for 100% ion yield, or 73 pg for 4% ion yield. Measurements on a single multiplier (duty cycle 10%) with ion yield of 4% would require 730 pg of Pb.

Now let us consider measurements on a Faraday cup array with 10^{11} Ohm resistor amplifiers. The precision of analyses (colored lines in Fig. 10) and the amount of Pb required for achieving the precision threshold depend on how the measurements are organized. In the following discussion, we assume 4% ion yield and 80% duty cycle (i.e., 20% of time is spent on focusing, peak centering, and intensity adjustments), and the baseline is measured outside the time of optimal ion emission (e.g., during sample warm-up). If we could maintain and measure the ion beam for 10 min, and measure the baseline for 10 min, we could get the required precision from 247 pg of Pb. If, however, we measure at lower intensity for a longer time (60 min), we would require 954 pg of Pb, almost

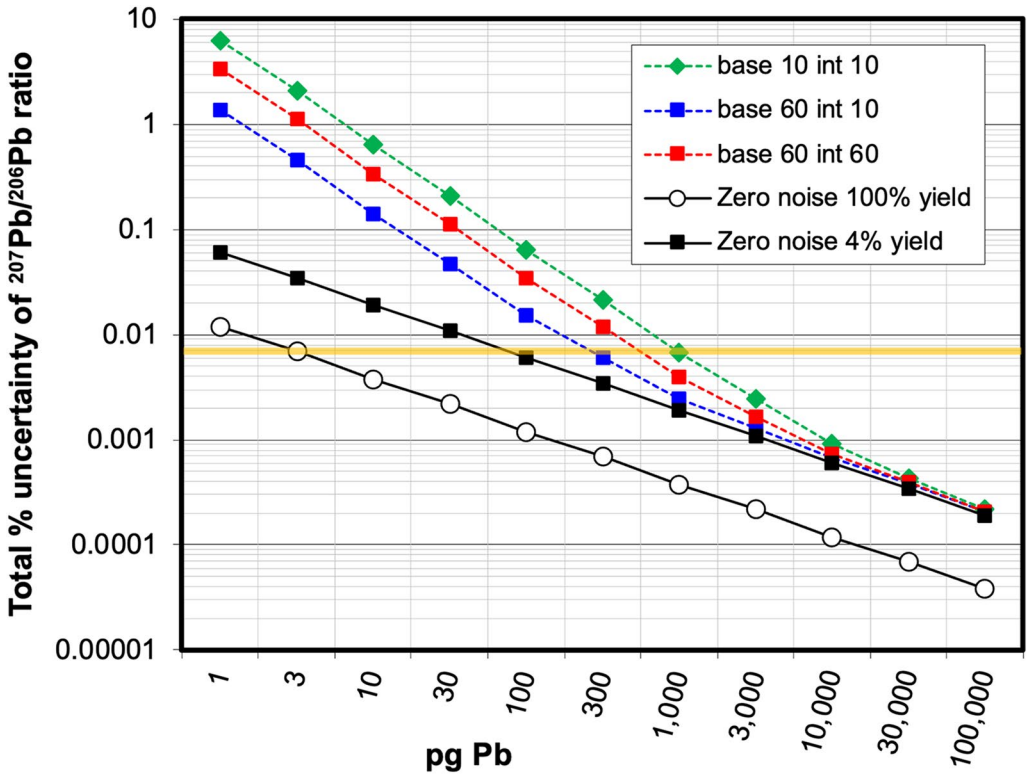

Fig. 10 Theoretical relative uncertainties (2σ) of $^{207}Pb/^{206}Pb$ ratios in Pb with atomic abundances of $^{206}Pb = 25\%$ and $^{207}Pb = 15.5\%$ (corresponding to $^{207}Pb/^{206}Pb = 0.62$, a radiogenic isotope composition for a 4555 Ma material) for total amount of Pb from 1 pg to 100 ng. The black lines "zero noise 100% yield" and "zero noise 4% yield" show uncertainties of static multicollector measurements based on counting statistics only, calculated using Eqs. 6–8 and assuming total ion yields of 100% and 4%, respectively. Black dashed line shows uncertainties of peak jumping measurements on a single ion counting multiplier (ion yield 4%, measurement duty cycle 10%, zero amplifier noise). The three colored dashed lines show uncertainties calculated using Eq. 9 and assuming amplifier noise of 4×10^{-16} A/s (equal to Johnson–Nyquist noise for amplifiers with 10^{11} Ohm resistors) and various times of baseline measurement (base) and signal integration (int) in minutes. The noise-related uncertainty components are calculated using Eqs. 10–11. For all calculations, it is assumed that the ion beam intensity remained constant during analysis, and that signal integration occupied 80% of the total measurement time (duty cycle 80%). The baseline is assumed to be measured outside the useful emission time (e.g., during warmup). The horizontal orange line shows the significance threshold adopted in this study

four times more than in the previous case. The dark noise on the peaks is becoming a significant contributor to the total uncertainty. By taking a longer baseline measurement (60 min on peak, 60 min baseline), we reduce the background uncertainty, and can get the desired precision from 532 pg of Pb. The choice of short (10 min), high intensity signal acquisition and long (60 min) baseline measurement gives the best effective sensitivity: the required sample size is 202 pg.

Measurements with an instrument with low-noise amplifiers (6.15×10^{-17} A/s, equal to 0.15 of Johnson–Nyquist noise for amplifiers with 10^{11} Ohm resistors, and representing noise performance of ATONA amplifiers, Additional file 1: Table S3), shown with red lines in Fig. 11, allow to achieve the same precision from substantially smaller samples. For the combination of long signal acquisition and short baseline, which is most sensitive to the amplifier noise, using a mass spectrometer with low-noise amplifiers allow us to measure ca. five times smaller samples (187 pg vs. 954 pg). For the combination of short signal acquisition and long baseline, the advantage of using a low-noise instrument is smaller but still significant (94 pg vs. 202 pg). In this case, the required sample size for a measurement on a low-noise instrument is only slightly larger for a measurement with a completely noise-free multicollector instrument.

Noise modeling described above shows that both the amplifier noise and the design of analysis are similarly important. In order to achieve the best precision, we have to optimize both parameters. It is also important to be able to measure the baseline outside the time of optimal emission. This would allow us to minimize the contribution of background uncertainty to the total uncertainty without compromising duty cycle. Baseline measurements can be carried out during sample filament warmup, or even overnight, if the amplifier baselines are free

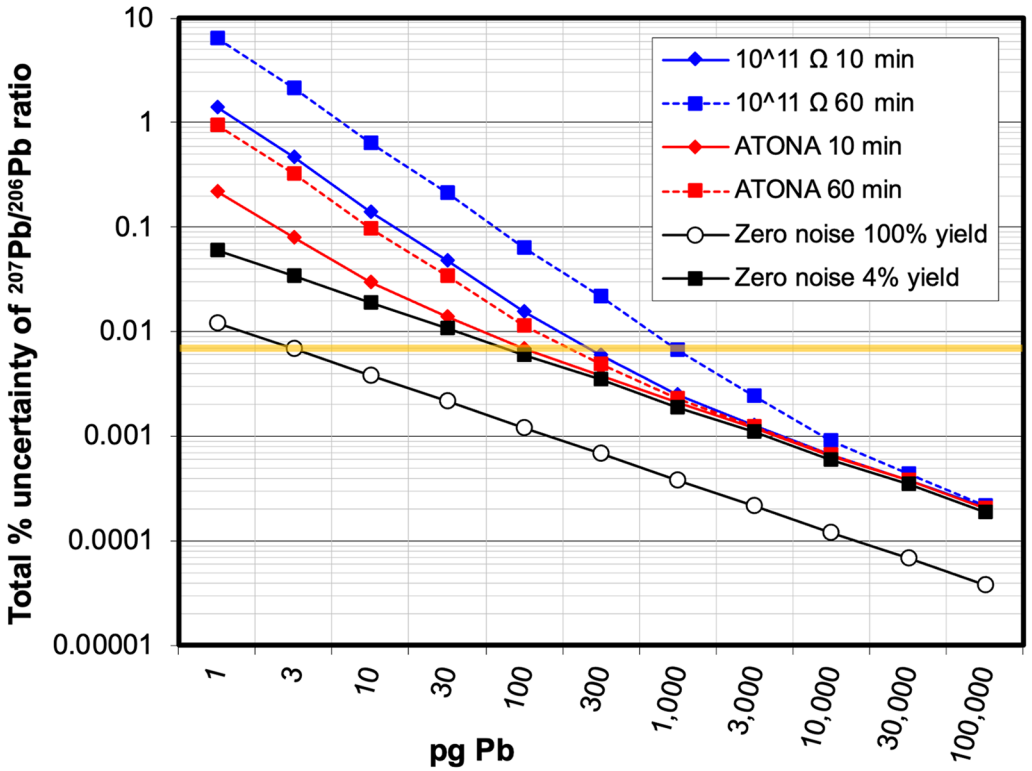

Fig. 11 Comparison of theoretical relative uncertainties (2σ) for Pb isotope analysis using amplifiers with noise of 4×10^{-16} A/s (equal to Johnson–Nyquist noise for amplifiers with 10^{11} Ohm resistors; blue lines), and amplifiers with noise of 6.15×10^{-17} A/s (equal to 0.15 of Johnson–Nyquist noise for amplifiers with 10^{11} Ohm resistors, and representing noise performance of ATONA amplifiers shown in Additional file 1: Table S2; red lines). Solid curves with smaller symbols correspond to 10-min signal integrations, dashed curves with larger symbols—to 60-min integrations. Baseline measurement time is 10 min in all cases. All other parameters are the same as in Fig. 10

from long-term drift and fluctuations that exceed the noise.

Measured versus theoretical uncertainties for ancient radiogenic Pb

In Fig. 12, precision of Pb isotope analysis in angrites and reference material SRM 981, measured in static multicollector mode on the Triton at the Geological Survey of Canada in 2003–2007, is compared to the theoretical uncertainty values modeled in Additional file 1: Table S4. The two theoretical curves represent measurements on a mass spectrometer with baseline noise equal to Johnson–Nyquist of 10^{11} Ohm resistors, ion yield 4%, baseline integration time 30 min, signal measurement time either 10 min or 60 min, and duty cycle of 80%. These parameters closely approximate the actual analytical conditions. There is generally a good agreement between modeled and measured precision, as most data plot between the two theoretical curves. Some points, however, are below the curve corresponding to 10-min signal measurement. Unusually high precision of these analyses can be caused by two reasons. Firstly, some samples produced higher total ion yields reaching 8–9%, about twice as high as the average value of 4% applied in the model. Secondly, higher precision can be a result of weighing by precision in calculation of the mean values of fractionation corrected $^{207}Pb/^{206}Pb$ ratios (Amelin and Davis 2006). If the filament current is continuously increased, then there is relatively short period in the middle of the run where the intensity is the highest, and the within-block uncertainty is the lowest (see Fig. 1 in Amelin and Davis 2006). These high-intensity blocks dominate calculation of the weighted mean $^{207}Pb/^{206}Pb$ ratios and their uncertainties, and short duration of this part of the run reduces the dark noise on the peak, in the same way as shown in Figs. 10 and 11 for modeled uncertainties.

The best thermal ionization mass spectrometer

In this section, I do not discuss a hypothetical perfect mass spectrometer and do not compare instruments offered by various manufacturers. Instead, I am trying to imagine a design most suitable for precise U–Pb geochronology (and other types of isotope analysis with small to medium size ion beams) that could be achieved by a combination of existing technologies if competition

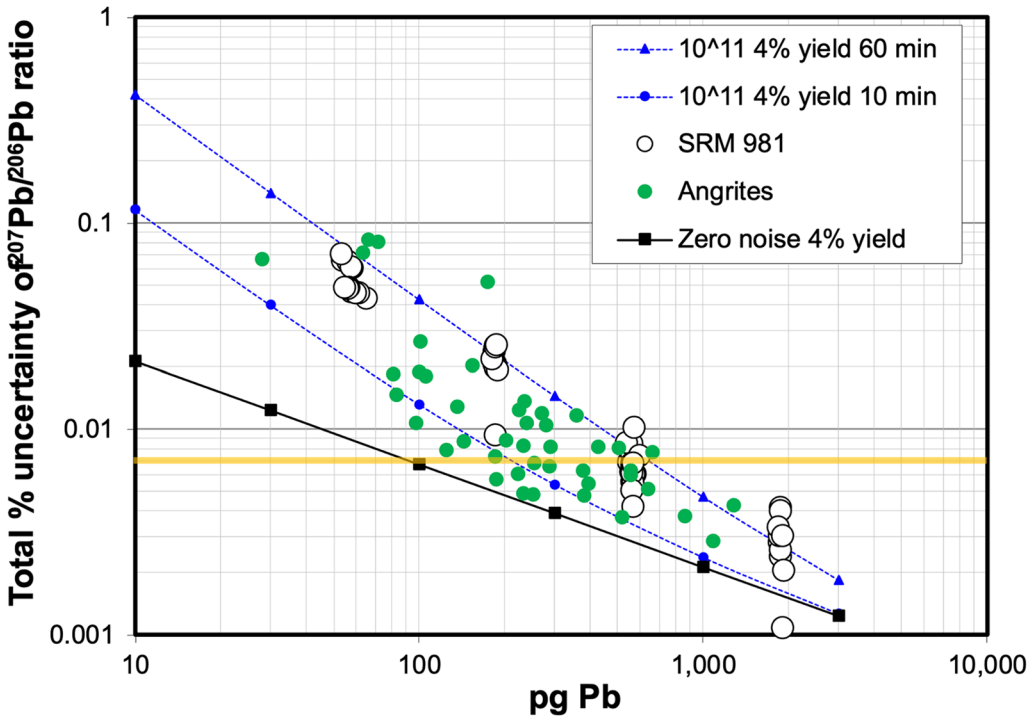

Fig. 12 Precision of Pb isotope analyses of angrites and reference material SRM 981 measured on the GSC Triton from Amelin and Davis (2006), Amelin (2008a, b), and Amelin et al. (2024), compared to theoretical noise level calculated as shown in Figs. 10 and 11 (baseline noise equal to Johnson–Nyquist of 10^{11} Ohm resistors, ion yield 4%, baseline integration time 30 min, signal measurement time either 10 min or 60 min, data acquisition occupies 80% of the total measurement time). The horizontal orange line shows the significance threshold

between the mass spectrometer manufacturers and patenting issues could be overcome (or disregarded), and a reasonable increase of the instrument cost (possibly bringing TIMS into the MC-ICPMS and MC-SIMS price range) could be tolerated.

1. The system should use multiple channels for simultaneous measuring of all isotopes of Pb—the reduction of duty cycle in single collector systems is inacceptable.
2. The system should use electrometer amplifiers connected to Faraday cups for measuring major isotopes of Pb. Problems with linearity, dynamic range and gain stability preclude using ion counters for this purpose.
3. The collector array should include one ion counting multiplier channel for measuring ^{204}Pb. Gain stability of this ion counter relative to electrometer channels should be good enough to allow measurements of ^{204}Pb with adequate accuracy in static mode with infrequent gain calibrations.
4. The electrometers should use technology that provides the lowest noise combined with fast response, wide dynamic range, and good long-term baseline stability. Charge collection such as implemented in Zeptona (and to a lesser degree ATONA) amplifiers seems to be the best currently available choice.
5. If it is confirmed that mechanical elements are indeed a significant source of noise at the level of Zeptona baseline as suggested above (section "Noise of ion detection systems"), then the system should be designed with an array of fixed collectors, and zoom ion optics for changing dispersion. The zoom should be tested for the absence of changes of channel gains with changing dispersion settings, such as those described above (section "Accuracy of the ion detection systems") for Triton Plus.

A mass spectrometer that combines all the above features is completely within the reach of the present-day technology. I hope that such an instrument will be available soon.

Summary and conclusions

In a hypothetical analytical setup that is free from noise, losses and biases, a sample containing 2.9 picograms of 4555 Ma radiogenic Pb would be sufficient to achieve precision of the $^{207}Pb/^{206}Pb$ ratio of 0.007% at 2σ level, corresponding to the $^{207}Pb^*/^{206}Pb^*$ age uncertainty of 0.1 Ma—the state of the art of precision in Pb-isotopic dating of ancient materials. With the best currently available techniques and instrumentation, we would need about 20–30 times larger amount of Pb. The main reason why larger samples are required is loss of Pb by evaporation from the filament as neutral atoms rather than ions. The other factor that deteriorates the precision versus sample size relationship is baseline noise of electrometer amplifiers, although, with the best existing low-noise amplifiers and optimum planning of signal acquisition, the contribution of baseline noise to the total uncertainty can be small compared to the counting statistics. Several factors unrelated to mass spectrometry, including uncertainties introduced by blank and spike subtraction, can also be significant.

Achieving a substantial increase in ionization efficiency of Pb, improvement of baseline stability, and reduction of analytical blanks are the key measures that could revolutionize Pb-isotopic dating and greatly expand its application range. Several other factors, such as losses and biases caused by sample leaching, and mass-independent isotopic fractionation in mass spectrometry, are currently less important, but can become significant parts of the total uncertainty as the required precision is pushed beyond today's state of the art.

Supplementary Information

The online version contains supplementary material available at https://doi.org/10.1186/s40543-024-00435-3.

Additional file 1. Table S1. Variations of calculated Pb isotopic ratios in the reference material EarlyTime 1x with assumed blank parameters. **Table S2**. Johnson-Nyquist noise at 24°C as a function of feedback resistance and integration time. **Table S3**. Comparison of amplifier noise in select mass spectrometers with theoretical (Johnson-Nyquist) noise of 10^{11} Ohm resistor at 24°C. **Table S4**. Precision of measurements of the 207Pb/206Pb by TIMS as a function of sample size, ion yield, baseline noise, and measurement conditions (integration times for signal and baseline).

Acknowledgements

This study has been inspired by the work of Ken Ludwig and fueled by discussions of analytical techniques of isotope geochemistry in general and U-Pb dating in particular, with many of my colleagues including, but not limited to Larry Heaman, Don Davis, Fernando Corfu, Sandra Kamo, Bill Davis, Leonid Neymark, Qingzhu Yin, Mini Wadhwa, Stein Jacobsen, Trevor Ireland, Vickie Bennett, Sonja Zink, Rick Carlson, Francois Tissot, Bruce Charlier, and Jim Connelly, as well as working together with former students and postdocs Tsuyoshi Iizuka, Magda Huyskens, Marian Sapah, Piers Koefoed, Renaud Merle, Evgenii Krestianinov, Yankun Di, and Chini Datta. Analytical data presented here were collected using TIMS at the Geological Survey of Canada, Australian National University, Korea Basic Science Institute, and Guangzhou Institute of Geochemistry. Completion of this work was possible due to support from the NRF Brain Pool program and hospitality of Keewook Yi and other colleagues at KBSI.

Author contributions

Sole author, hence not applicable.

Funding

Not applicable.

Availability of data and materials

Not applicable.

Declarations

Competing interests

The author declares no competing interests.

Received: 29 November 2023 Accepted: 3 April 2024
Published online: 23 April 2024

References

Amelin Y. U-Pb ages of angrites. Geochim Cosmochim Acta. 2008a;72(1):221–32.
Amelin Y. The U-Pb systematics of angrite Sahara 99555. Geochim Cosmochim Acta. 2008b;72(19):4874–85.
Amelin Y, Davis WJ. Isotopic analysis of lead in subnanogram quantities by TIMS using a 202Pb-205Pb spike. J Anal at Spectrom. 2006;21:1053–61.
Amelin Y, Krot AN. Pb isotopic age of the Allende chondrules. Meteorit Planet Sci. 2007;42:1321–35.
Amelin Y, Merle R. Isotopic analysis of potassium by total evaporation and incipient emission thermal ionisation mass spectrometry. Chem Geol. 2021;559:1199.
Amelin Y, Ghosh A, Rotenberg E. Unraveling evolution of chondrite parent asteroids by precise U-Pb dating and thermal modeling. Geochim Cosmochim Acta. 2005a;69:505–18.
Amelin Y, Davis DW, Davis WJ. Decoupled fractionation of even- and odd mass isotopes of Pb in TIMS. Geochim Cosmochim Acta. 2005b;69:A215.
Amelin Y, Connelly J, Zartman RE, Chen JH, Göpel C, Neymark LA. Modern U-Pb chronometry of meteorites: Advancing to higher time resolution reveals new problems. Geochim Cosmochim Acta. 2009;73:5212–23.
Amelin Y, Kaltenbach A, Iizuka T, Stirling CH, Ireland TR, Petaev M, Jacobsen SB. U-Pb chronology of the Solar System's oldest solids with variable $^{238}U/^{235}U$. Earth Planet Sci Lett. 2010;300(3):343–50.
Amelin Y, Koefoed P, Iizuka T, Fernandes VA, Huyskens MH, Yin Q-Z, Irving AJ. U-Pb, Rb-Sr and Ar-Ar systematics of the ungrouped achondrites Northwest Africa 6704 and Northwest Africa 6693. Geochim Cosmochim Acta. 2019;245:628–42.
Amelin Y, Huyskens MH. Performance of Pb multi ion counting array in triton plus TIMS. 2013 Goldschmidt Conference abstracts, #4047, 2013.
Amelin Y, Yin Q-Z, Koefoed P, Merle R, Hibiya Y, Huyskens MH, Iizuka T, Cartwright JA. Fractionation of radiogenic Pb isotopes in meteorites and their components induced by acid leaching. Geochim Cosmochim Acta, under revision, 2024.
Bigeleisen J. Nuclear size and shape effects in chemical reactions; isotope chemistry of the heavy elements. J Am Chem Soc. 1996;118:3676–80.
Birck JL. The precision and sensitivity of thermal ionisation mass spectrometry (TIMS): an overview of the present status. Geostand Newsl. 2001;25(2–3):253–9.
Blichert-Toft J, Zanda B, Ebel DS, Albarède F. The Solar System primordial lead. Earth Planet Sci Lett. 2010;300:152–63.
Bollard J, Connelly JN, Whitehouse MJ, Pringle EA, Bonal L, Jørgensen JK, Nordlund Å, Moynier F, Bizzarro M. Early formation of planetary building blocks inferred from Pb isotopic ages of chondrules. Sci Adv. 2017;3: e170040.
Callis EL, Abernathey RM. High-precision isotopic analyses of uranium and plutonium by total sample evaporation and signal integration. Int J Mass Spectrom Ion Process. 1991;103:93–105.

Carlson RW. Thermal ionization mass spectrometry. In: Treatise on Geochemistry 2nd Edition, Chapter 15.18; 2014. pp. 337–354.
Compston W, Oversby VM. Lead isotopic analysis using a double spike. J Geophys Res. 1969;74(17):4338–48.
Condon DJ, Schoene B, McLean NM, Bowring SA, Parrish R. Metrology and traceability of U-Pb isotope dilution geochronology (EARTHTIME Tracer Calibration Part I). Geochim Cosmochim Acta. 2015;164:464–80.
Connelly JN, Bizzarro M. Pb–Pb dating of chondrules from CV chondrites by progressive dissolution. Chem Geol. 2009;259:143–51.
Connelly JN, Bizzarro M, Krot AN, Nordlund Å, Wielandt D, Ivanova MA. The absolute chronology and thermal processing of solids in the solar protoplanetary disk. Science. 2012;338:651–5.
Connelly JN, Bollard J, Bizzarro M. Pb–Pb chronometry and the early Solar System. Geochim Cosmochim Acta. 2017;201:345–63.
Connelly JN, Bollard J, Costa MM, Vermeesch P, Bizzarro M. Improved methods for high-precision Pb–Pb dating of extra-terrestrial materials. J Anal at Spectrom. 2021;36:2579–87.
Connelly JN, Bollard J, Amsellem E, Schiller M, Larsen KK, Bizzarro M. Evidence for very early planetesimal formation and $^{26}Al/^{27}Al$ heterogeneity in the protoplanetary disk. Astrophys J Lett. 2023;952:L33.
Davis DW. (2020) A simple method for rapid calibration of faraday and ion-counting detectors on movable multicollector mass spectrometers. J Mass Spectrom. 2020;55: e4511.
Davis DW, Krogh TE. Preferential dissolution of ^{234}U and radiogenic Pb from alpha-recoil-damaged lattice sites in zircon; implications for thermal histories and Pb isotopic fractionation in the near surface environment. Chem Geol. 2000;172:41–58.
Davis AM, Richter FM, Mendybaev RA, Janney PE, Wadhwa M, McKeegan KD. Isotopic mass fractionation laws for magnesium and their effects on ^{26}Al–^{26}Mg systematics in solar system materials. Geochim Cosmochim Acta. 2015;158:245–61.
Di Y, Li Z, Amelin Y. Monitoring and quantitative evaluation of Faraday cup deterioration in a thermal ionization mass spectrometer using multidynamic analyses of laboratory standards. J Anal at Spectrom. 2021;36:1489–502.
Dodson MH. A theoretical study of the use of internal standards for precise isotopic analysis by the surface ionization technique: Part I—General first-order algebraic solutions. J Sci Instrum. 1963;40:289.
Doucelance R, Manhès G. Reevaluation of precise lead isotope measurements by thermal ionization mass spectrometry: comparison with determinations by plasma source mass spectrometry. Chem Geol. 2001;176:361–77.
Esat TM. A 61 cm radius multi-detector mass spectrometer at the Australian National University. Nucl Inst Methods Phys Res B. 1984;5:545–53.
Esat TM. Charge collection thermal ionization mass spectrometry of thorium. Int J Mass Spectrom Ion Process. 1995;148:159–70.
Gaynor SP, Ruiz M, Schaltegger U. The importance of high precision in the evaluation of U-Pb zircon age spectra. Chem Geol. 2022;603: 120913.
Gerstenberger H, Haase G. A highly effective emitter substance for mass spectrometric Pb isotope ratio determinations. Chem Geol. 1997;136:309.
Guseva LI. A study of ion-exchange behavior of Pb in dilute HBr solutions, aimed to evaluate the possibility of on-line isolation of element 114. 228Ra-212Pb generator. Radiochemistry. 2007;49:92–6.
Hart SR, Zindler A. Isotopic fractionation laws: a test using calcium. Int J Mass Spectrom Ion Process. 1989;89:287–301.
Hockley M, Palacz Z, Yardley S, Jones T. Ultra low noise and baseline drift Zeptona Faraday detector. IsotopX Technical Note 2102; 2021. https://www.isotopx.com/resources/ultra-low-noise-and-baseline-drift-zeptona-faraday-detector
Holmden C, Bélanger N. Ca isotope cycling in a forested ecosystem. Geochim Cosmochim Acta. 2010;74:995–1015.
Huyskens MH, Iizuka T, Amelin Y. Evaluation of colloidal silicagels for lead isotopic measurements using thermal ionisation mass spectrometry. J Anal at Spectrom. 2012;27(9):1439–46.
Huyskens MH, Zink S, Amelin Y. Evaluation of temperature-time conditions for the chemical abrasion treatment of single zircons for U-Pb geochronology. Chem Geol. 2016;438:25–35.
Ireland TR, Schram N, Holden P, Lan P, Ávila J, Armstrong R, Amelin Y, Latimore A, Corrigan D, Clement S, Foster JJ, Compston W. Charge mode electrometer measurements of S-isotopic compositions on SHRIMP-SI. Int J Mass Spectrom. 2014;359:26–37.
Johnson JB. Thermal agitation of electricity in conductors. Phys Rev. 1928;32:97–109.
Kamber BS, Gladu AH. Comparison of Pb purification by anion-exchange resin methods and assessment of long-term reproducibility of Th/U/Pb ratio measurements by quadrupole ICP-MS. Geostand Geoanalytical Res. 2009;33(2):169–81.
Koornneef J, Bouman C, Schwieters J, Davies G. Measurement of small ion beams by thermal ionisation mass spectrometry using new 10^{13} Ohm resistors. Anal Chim Acta. 2014;819:49–55.
Korkisch J, Hazan I. Anion-exchange separations in hydrobromic acid-organic solvent media. Anal Chem. 1965;37:707–10.
Krestianinov E, Amelin Y, Yin Q-Z, Cary P, Huyskens MH, Miller A, Dey S, Hibiya Y, Tang H, Young ED, Pack A, Di Rocco T. Igneous meteorites suggest Aluminium-26 heterogeneity in the early Solar Nebula. Nat Commun. 2023;14:4940.
Krogh TE. A low-contamination method for hydrothermal decomposition of zircon and extraction of U and Pb for isotopic age determinations. Geochim Cosmochim Acta. 1973;37:485–94.
Low Level Measurements Handbook, Keithley Corporation. Keithley Instruments, pp. 244; 2004. http://www.valtar.ru/Manuals/Precis/LLMsH_06.pdf
Ludwig KR. Optimization of multicollector isotope-ratio strontium and neodymium. Chem Geol. 1997;135:325–34.
Ludwig KR. Constraints on time-efficient data-taking strategies for single-collector, isotope ratio mass spectrometers. In: Shorter Contributions to Isotope Research, U.S. Geological Survey Bulletin 1622; 1986.
Mattinson JM. Zircon U-Pb chemical abrasion ("CA–TIMS") method: combined annealing and multi-step dissolution analysis for improved precision and accuracy of zircon ages. Chem Geol. 2005;220(1–2):47–66.
Mattinson JM. Extending the Krogh legacy: development of the CA–TIMS method for zircon U-Pb geochronology. Can J Earth Sci. 2011;48:95–105.
McLean NM, Condon DJ, Schoene B, Bowring SA. Evaluating uncertainties in the calibration of isotopic reference materials and multi-element isotopic tracers (EARTHTIME Tracer Calibration Part II). Geochim Cosmochim Acta. 2015;164:481–501.
Merle R, Amelin Y, Yin Q-Z, Huyskens MH, Sanborn ME, Nagashima K, Yamashita K, Ireland TR, Krot AN, Sieber MJ. Exploring the efficiency of stepwise dissolution in removal of stubborn non-radiogenic Pb in chondrule U-Pb dating. Geochim Cosmochim Acta. 2020;277:1–20.
Mundil R, Ludwig KR, Metcalfe I, Renne PR. Age and timing of the Permian mass extinctions. Science. 2004;305(5691):1760–3.
Nyquist H. Thermal agitation of electric charge in conductors. Phys Rev. 1928;32:110–3.
Palacz Z, Jones T, Toote D, Guest R, Locke S. Performance characteristics of an enhanced Daly ion counting system for TIMS. Min Mag. 2011;75:1588.
Parrish RR, Krogh TE. Synthesis and purification of ^{205}Pb for U-Pb geochronology. Chem Geol. 1987;66:103–10.
Richter S, Goldberg S, Mason P, Traina A, Schwieters J. Linearity tests for secondary electron multipliers used in isotope ratio mass spectrometry. Int J Mass Spectrom. 2001;206:105–27.
Russell WA, Papanastassiou DA, Tombrello TA. Ca isotope fractionation on the Earth and other solar system materials. Geochim Cosmochim Acta. 1978;42:1075–90.
Schaltegger U, Schmitt AK, Horstwood MSA. U-Th–Pb zircon geochronology by ID-TIMS, SIMS, and laser ablation ICP-MS: recipes, interpretations, and opportunities. Chem Geol. 2015;402:89–110.
Schaltegger U, Ovtcharova M, Gaynor SP, Schoene B, Wotzlaw J, Davies JHFL, Farina F, Greber N, Szymanowski D, Chelle-Michout C. Long-term repeatability and interlaboratory reproducibility of high-precision ID-TIMS U-Pb geochronology. J Anal at Spectrom. 2021;36:1466–77.
Schmitz MD, Schoene B. Derivation of isotope ratios, errors, and error correlations for U-Pb geochronology using ^{205}Pb-^{235}U-(^{233}U)-spiked isotope dilution thermal ionization mass spectrometric data. Geochem Geophys Geosyst. 2007;8:Q08006. https://doi.org/10.1029/2006GC001492.
Schoene B. U-Th-Pb geochronology. In: Treatise on Geochemistry 2nd Edition, Chapter 4.10; 2014. pp. 341–378.
Strelow FWE, von Toerien FS. Separation of lead(II) from bismuth(III), thallium(III), cadmium(III), mercury(II), gold(III), platinum(IV), palladium(II), and other elements by anion exchange chromatography. Anal Chem. 1966;38:545–8.
Szymanowski D, Schoene B. U-Pb ID-TIMS geochronology using ATONA amplifiers. J Anal at Spectrom. 2020;35:1207–16.

Tatsumoto M, Knight RJ, Allègre CJ. Time differences in the formation of meteorites as determined from the ratio of Lead-207 to Lead-206. Science. 1973;180:1279–83.
Thirlwall MF. Inter-laboratory and other errors in Pb isotope analyses investigated using a ^{207}Pb-^{204}Pb double spike. Chem Geol. 2000;163(1–4):299–322.
Todt W, Cliff RA, Hanser A, Hofmann A. Evaluation of a ^{202}Pb–^{205}Pb double spike for high-precision lead isotope analysis. Geophys Monogr. 1996;95:429–37.
Vermeesch P. IsoplotR: a free and open toolbox for geochronology. Geosci Front. 2018;9:1479–93. https://doi.org/10.1016/j.gsf.2018.04.001.
von Quadt A, Wotzlaw J-F, Buret Y, Large SJ, Peytcheva I, Trinquier A. High-precision zircon U/Pb geochronology by ID-TIMS using new 10^{13} Ohm resistors. J Anal at Spectrom. 2016;31(3):658–65.
Wasserburg GJ, Tera F, Papanastassiou DA, Huneke JC. Isotopic and chemical investigations of Angra dos Reis. Earth Planet Sci Lett. 1977;35:294–316.
Wimpenny J, Sanborn ME, Koefoed P, Cooke IR, Stirling C, Amelin Y, Yin Q-Z. Reassessing the origin and chronology of the unique achondrite Asuka 881394: Implications for distribution of ^{26}Al in the early Solar System. Geochim Cosmochim Acta. 2019;244:478–501.
Yokoyama T, Makishima A, Nakamura E. Evaluation of the coprecipitation of incompatible trace elements with fluoride during silicate rock dissolution by acid digestion. Chem Geol. 1999;157:175–87.
Zhou C, Huyskens MH, Lang X, Xiao S, Yin Q-Z. Calibrating the terminations of Cryogenian global glaciations. Geology. 2019;47(3):251–4.
Zou H. Error propagation. In: Treatise on Geochemistry, chapter 15.2; 2014. pp 33–42.

Publisher's Note

Springer Nature remains neutral with regard to jurisdictional claims in published maps and institutional affiliations.